ELSEVIER

Journal of Structural Geology 28 (2006) 1445–1467

JOURNAL OF STRUCTURAL GEOLOGY

www.elsevier.com/locate/jsg

Architecture and deformation mechanism of a basin-bounding normal fault in Mesozoic platform carbonates, central Italy

Fabrizio Agosta*, Atilla Aydin

Rock Fracture Project, Department of Geological and Environmental Sciences, Stanford University, Stanford, CA 94305-2115, USA

Received 6 December 2005; received in revised form 30 March 2006; accepted 5 April 2006
Available online 12 July 2006

Abstract

We studied the mechanisms and intensity of deformation across a large, active, basin-bounding normal fault zone in Mesozoic platform carbonates. Based on the modes, orientation, crosscutting and abutting relationships of various structural elements preserved within the fault zone and in the surrounding host rocks, we propose a conceptual model of normal fault growth under an extensional tectonic regime that follows an earlier contractional regime. Normal faults initiated by shearing of the pre-existing elements, predominantly pressure solution seams inherited from the contractional regime, formation and subsequent shearing of new seams and joints/veins, and localization of pods of fragmented carbonates within the individual mechanical layers. With ongoing deformation and emersion from depth, two sets of conjugate normal faults developed within the fault zone through the fragmented pods. The end result is normal fault zone with a maximum of 600 m of throw that includes deformed basinal sediments in the hanging wall, and up to 1-m thick fault core and 100-m thick damage zone in the footwall. The fault core is made up of matrix-supported and cement-supported fault rocks and major slip surfaces. The damage zone consists of small faults and fragmented carbonates; the intensity of deformation generally increases towards the fault core.

Keywords: Platform carbonates; Failure modes; Normal fault growth; Fault architecture; central Apennines

1. Introduction

Fault zones have two compartments: core and damage zones (Chester et al., 1993; Antonellini and Aydin, 1994; Caine et al., 1996). The fault core includes fault rocks that develop around the major slip surfaces due to comminution, dissolution/precipitation, mineral reactions, and other mechanical and chemical processes that destroy the fabric of the host rock (Sibson, 1977; Chester and Logan, 1986). The damage zone flanks the fault core and consists of a wider zone of fractures and smaller faults that do not completely obliterate the host rock fabric (Cowie and Scholz, 1992). Both core and damage zones are surrounded by the host rock, which has a background value of deformation intensity. Characterization of both deformation mechanisms and structural elements that characterize the fault zones is crucial to understanding the processes of fault growth (Martel et al., 1988; Davatzes and Aydin, 2003; Myers and Aydin, 2004) and fault architecture and permeability (Caine et al., 1996; Aydin, 2000).

Faulting in carbonate rocks involves the sequential formation and shearing of joints, veins, and/or pressure solution seams (Alvarez et al., 1978; Marshak et al., 1982; Peacock and Sanderson, 1995; Kelly et al., 1998; Salvini et al., 1999). Three main deformation mechanisms along faults in carbonates have been documented in some detail. Strike-slip faulting in the dolomitic rocks of the Sella Group, in northern Italy, was initiated by echelon joints that were later sheared producing cross joints, which broke up the joint-bounded bridges and eventually formed throughgoing slip surfaces and fault breccia (Mollema and Antonellini, 1999). In another case, normal faults within the platform carbonates at the front of the Maiella thrust sheet in central Italy developed entirely

* Corresponding author. Tel.: +1 650 723 4788.
E-mail address: bizio@pangea.stanford.edu (F. Agosta).

0191-8141/$ - see front matter © 2006 Elsevier Ltd. All rights reserved.
doi:10.1016/j.jsg.2006.04.006

by a pressure solution-based mechanism (Graham et al., 2003). There, normal faults started with the shearing of the pre-existing bed-parallel and bed-perpendicular pressure solution seams, producing oblique pressure solution seams in their contractional quadrants. The interaction of these tail seams with the pre-existing bed-perpendicular seams fragmented the carbonate host rocks into isolated blocks that localized within adjacent mechanical layers. As deformation continued, the isolated blocks were eventually linked together by throughgoing breccia and slip surfaces. The third main mechanism was proposed for strike-slip faults in the shallow water, basinal carbonates of Somerset, UK (Willemse et al., 1997), involving both of the fundamental failure modes described above for the first, opening mode, and second, closing mode, mechanisms. Strike-slip faulting began with echelon veins that localized pressure solution within the vein-bounded bridges or at the contractional quadrants of the sheared veins. The bridges, or thin rock slabs, progressively rotated as deformation progressed, resulting in the shearing of the pressure solution seams, and the ongoing formation and shearing of the next generations of pressure solution seams and joints.

The Venere normal fault zone, which bound the southeastern side of the Fucino Basin in central Italy, provides an excellent opportunity to examine the sequence of a series of complex deformation mechanisms and the resulting fault architecture in platform carbonates. We document the development of a minimum of 10 km long normal fault in Mesozoic carbonates under an extensional regime that followed an earlier contractional regime. Agosta et al (in press) documented the higher values of both porosity and permeability of the fragmented carbonates, and their different pore structure, of the damage zones bounding the southeastern side of the Fucino basin relative to both host and fault rocks. Here, we identify the modes of fracturing and quantify the intensity and distribution of the deformation across the carbonate footwall of the Venere fault zone. This was accomplished by laboratory analyses of rock samples collected in the field, scanline measurements, characterization of the deformation background of the Mesozoic platform carbonates, and detailed mapping of the structural elements along the walls of quarries that entirely expose the Venere fault footwall for examination in three dimensions. Based on the pattern, distribution, crosscutting and abutting relationships of several sets of pressure solution seams, joints, veins, and cataclastic shear bands, we propose a conceptual model of normal fault growth and discuss our data in terms of carbonate deformation during ongoing normal faulting and exhumation from depth.

2. Methodology

Geological and fault maps (1:10,000 scale) were constructed from topographic and ortho-rectified aerial photographs to characterize the extensional relay area bounded by the Celano-Pescina-Parasano and Venere-Sperone fault systems (Fig. 1a). The internal fault strands and structural elements of the Venere fault zone were similarly mapped at 1:2000 and 1:5000 scale. Detailed documentation of the modes, distribution, crosscutting and abutting relationships

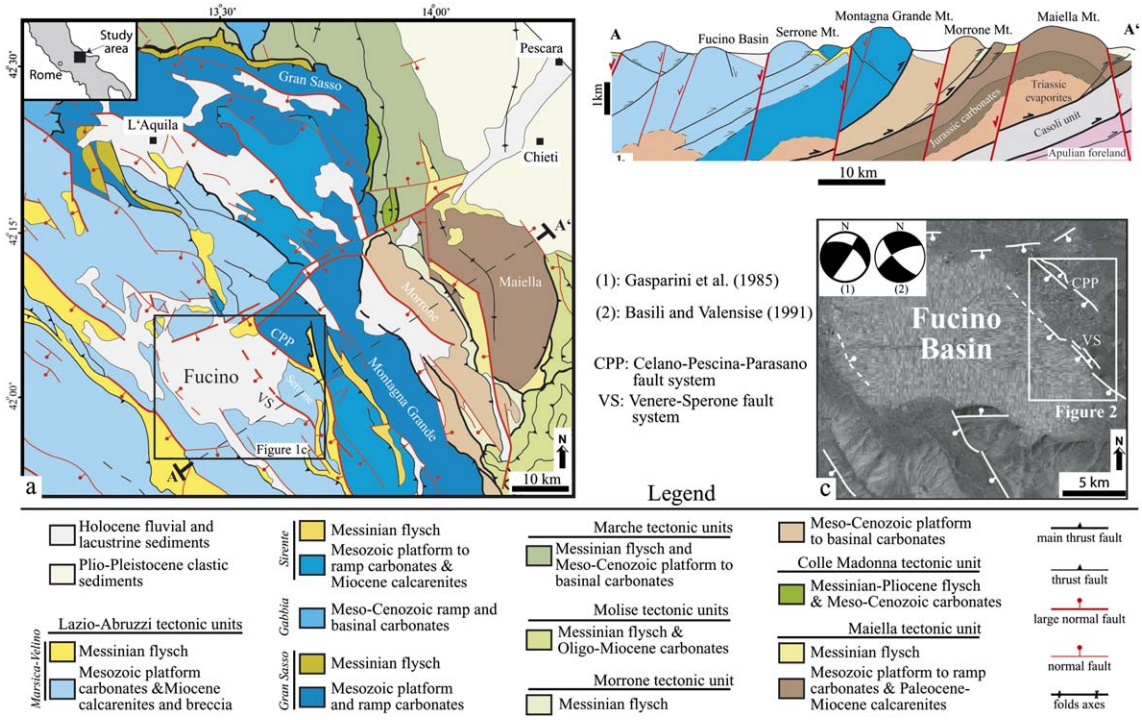

Fig. 1. (a) Simplified tectonic map of the Abruzzo region, central Italy (after Vezzani and Ghisetti, 1998). (b) NE–SW orientated, A–A′ simplified geological section across the southeastern portion of the Abruzzo region (see dashed line in a). (c) Trace of the normal fault scarps present in the Fucino area. The two published focal mechanisms of the 1915 Avezzano Earthquake are given in the inset. The rectangle outlines the relay ramp area bounded by the CPP and VS fault systems. See refs Gasparini et al., 1985 and Basili and Valensise, 1991.

of the faults and fractures present in the damage zone of the Venere fault footwall was made using ground photo mosaics, string line mapping, and by taping acetate sheets to the outcrops. This methodology allowed us to determine the relative ages of the structures and their role in the growth of the normal fault zone. The attitude of the planar elements presented in this paper is given according to the down-plunge direction (Twiss and Moores, 1992).

The intensity of deformation within the damage zone was quantified by scanline measurements of the fractures along the less deformed outcrops of an active quarry, and by conventional sieving-and-weighting of representative materials (Krumbein and Pettijohn, 1938). Rock samples were collected after removing 10–15 cm of weathered outcrop material, disaggregated in a non-destructive ultrasonic device, and sieved through nine sieves with standard mesh apertures ranging from 16.0 to 0.063 mm. The dry residue in each sieve was weighted in a precision balance with a resolution of 0.01 g. The number of equivalent spherical grains for each size class was determined by dividing the weight of the residue in each sieve by the weight of a sphere of 2670 kg/m^{-3}, the density of platform carbonates, and radius equal to half the mesh aperture of the next larger sieve (Storti et al., 2003). The residue in the sieve with the largest mesh aperture, 16.0 mm, was not considered to avoid any possible bias of the distribution towards coarser grains. Seven class sizes were therefore represented in the grain size distribution plots.

3. Geological setting and eastern boundary faults of the Fucino Basin

The Fucino Basin is in the Peri-Adriatic outer belt of the Apennines in central Italy, which has been termed as Central Apennines Downfaulted Area (CADA, Ghisetti and Vezzani, 1999). The CADA is characterized by NW trending normal faults that crosscut the contractional edifice of the Apennine fold and thrust belt (Bigi et al., 1992). These normal faults have been active since the Late Pliocene/Early Pleistocene (Bosi and Messina, 1991) during regional uplift and gravitational collapse (Ghisetti and Vezzani, 1999). The regional uplift rates calculated for the outermost portions of CADA, the Maiella Mountain, vary between 1.4 and 2.5 mm/yr since 3.5 and 1.6 Ma, respectively (Ghisetti and Vezzani, 1999). The largest normal faults of CADA flank continental basins (Fig. 1a and b). One of these, the Fucino Basin, is rhomb-shaped, ~30 km wide, and is filled with Late Pliocene-Holocene fluvio-lacustrine sediments (Bosi et al., 1995; Cavinato et al., 2002). The Fucino Basin is now floored by a flat plain due to the draining of what was once a natural lake, first by the ancient Romans (~50 AD) and again by the Torlonia Prince in 1875 (Giraudi, 1989).

The Fucino Basin is a half-graben bounded on the eastern side by two major structural lineaments (Fig. 1a): the Celano-Pescina-Parasano fault system (CPP), on the northeast, which is also known as the Marsicana Highway fault (Galadini and Galli, 1999); and the Venere-Sperone fault system (VS) on the southeast, also known as the Serrone (Piccardi et al., 1999; Cavinato et al., 2002) or San Benedetto-Gioia dei Marsi fault (Galadini and Galli, 1999). These two structural lineaments juxtapose the Quaternary basinal sediments against the Upper Jurassic-Lower Cretaceous massive platform carbonates of the Lazio-Abruzzi tectonic unit. The Mesozoic carbonates, about 1200 m thick, are boundstones with less than 1% porosity (Agosta et al., in press) unconformably overlain by hundreds of meters thick Middle Miocene carbonate grainstones and Messinian flysch (Vezzani and Ghisetti, 1998).

Active tectonics have created many geomorphic features, such as triangular facets and fault scarps, present along the mountain fronts and in the adjacent Fucino basinal sediments, respectively (Fig. 1c). The CPP and VS fault systems ruptured during the Avezzano earthquake of 1915 (Ms = 7.0, Boschi et al., 1997), producing ground cracks 0.3–1 m wide and fault scarps up to 1 m high in the continental sediments (Oddone, 1915). The rupture also exposed continuous, steep, ribbon-shaped scarplets in light-colored platform carbonates under the slope debris and basin-filling sediments (the 'nastro di faglia' of Bosi, 1975). The focal mechanism solutions of the earthquake recorded during this seismic event are consistent with oblique extension with a sub-horizontal T-axis oriented either E–W or NNE–SSE (inset of Fig. 1c), whereas trench investigations indicated pure normal faulting (Micchetti et al., 1996). Overall, an average throw slip rate of 0.4 to 1.0 mm/year and a minor right-lateral component have been documented in the Fucino area by the analysis of widespread fault scarps (Piccardi et al., 1999).

The CPP and VS fault systems form a kilometric extensional relay ramp dissected by several shorter, NW-striking normal faults sub-parallel to the major segments (Fig. 2). These shorter normal faults flank NW oriented, narrow, structural depressions in which Lower Pliocene conglomerates and Holocene lacustrine sediments and/or Messinian flysch have been preserved. Based on the offsets of the Miocene carbonate grainstones, the average throw across the relay ramp is about 400 m. Within this area, there are also normal faults that strike ENE–WSW, which localize at the edges of the relay ramp, and N–S that are bounded by the NW striking faults.

4. Venere Fault Zone

The Venere normal fault zone is more than 10 km long, has a maximum of 600 m of throw (Cavinato et al., 2002), and penetrates the Apenninic belt down to about one third of the 30–35 km thick crust (Ghisetti and Vezzani, 1999 and references therein). The northwestern termination of the fault zone occurs within the basinal sediments; the exact location of this fault tip is not clearly shown. On the contrary, the southeastern tip of the fault veers to the east by ~40° before ending within the carbonates. In the southeast, north of the town of Gioia dei Marsi, the Venere fault zone forms an underlap zone with the Sperone fault zone (Fig. 2). This underlap zone is crosscut by three WNW-trending normal faults that are well defined by clear geomorphic expressions. The south-central part of the Venere fault zone (marked by the rectangle in Fig. 2) can be seen in detail in five quarries located

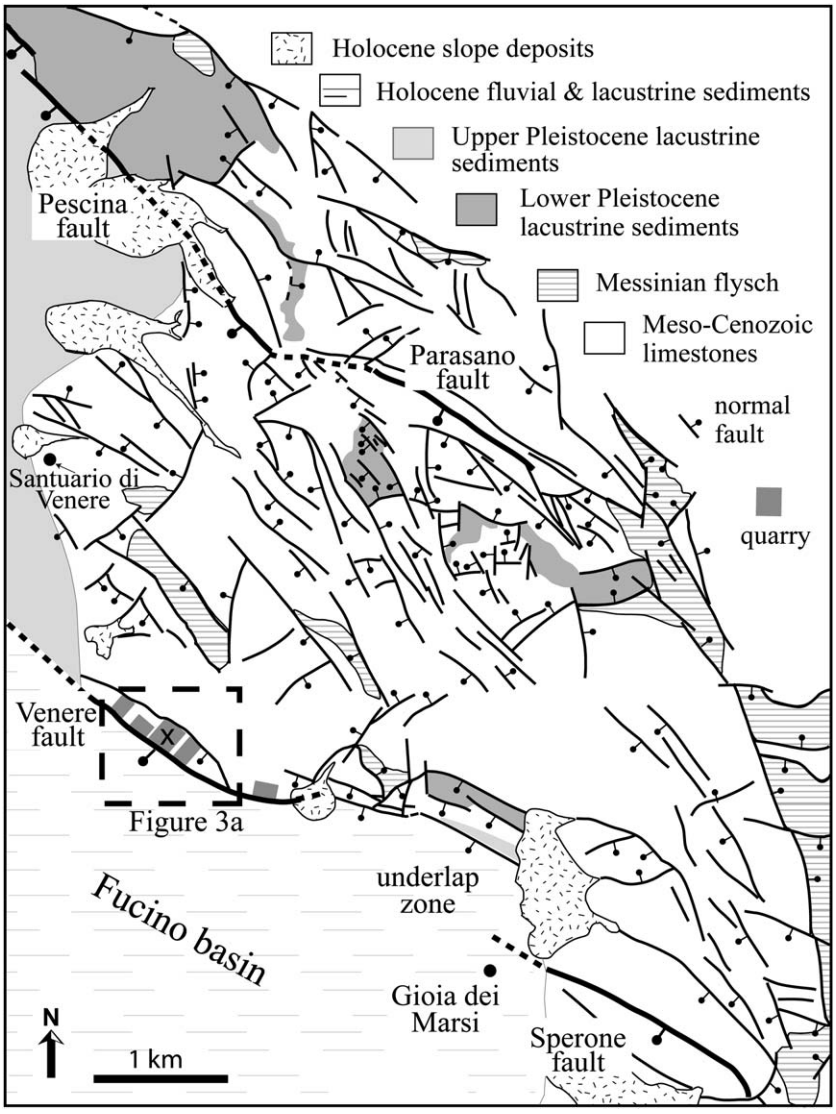

Fig. 2. Geological map of the relay ramp area bounded by the CPP and VS fault systems (cf. Fig. 1c). The footwall of the Venere fault is excavated by five quarries. The cross marks the location of the Santilli Quarry.

along the fault zone. We examined all five quarries for the presence and continuity of the fault components, but focused on the active Santilli Quarry, located at the ~13.1 km marker on road SS83, for detailed documentation (Fig. 3a).

In the hanging wall of the Venere fault zone, the Quaternary sediments dip either SW, towards the basin, or NE, towards Serrone Mountain, depending on segmentation, relative geometry, and the amount of slip of the fault panels at depth (Cartwright et al., 1995; Gawthorpe et al., 2003). Within the fault zone, the sediments and cemented slope scree of the hanging wall drape over, and are partly offset by, small faults with up to 16 cm of throw along the study outcrops. Locally, centimeter-thick slices of these sediments have been accreted into the footwall.

The footwall of the Venere fault zone is tilted towards the SW, as opposed to the consistent dip direction of the Mesozoic platform carbonates exposed throughout the Serrone Mountain, which is to the NE (Fig. 3a and b). The transition from the tilted footwall to the host rock with only a background amount of deformation is accommodated by a dip-slip fault that forms a distinctive scarp. The dip angle of the bedding in the platform carbonates within the fault zone varies from 20° SW to 65° SW, and is generally steeper nearer the hanging wall (Fig. 3b).

4.1. Fault core

Based on the continuous juxtaposition of the Quaternary sediments against the Mesozoic carbonates, we identified the first-order fault strand within the Venere fault zone (seen as the black and white double line in Fig. 3a). This major strand is composed of a fault core up to 1 m thick, which is laterally continuous along the study south-central portion of the fault zone and bounds the damage zone of the footwall (Fig. 3a). Based on the thickness of the fault core we estimate an offset of a few hundred meters along the first-order fault strand. The carbonate fault damage zone of the hanging wall, and possibly

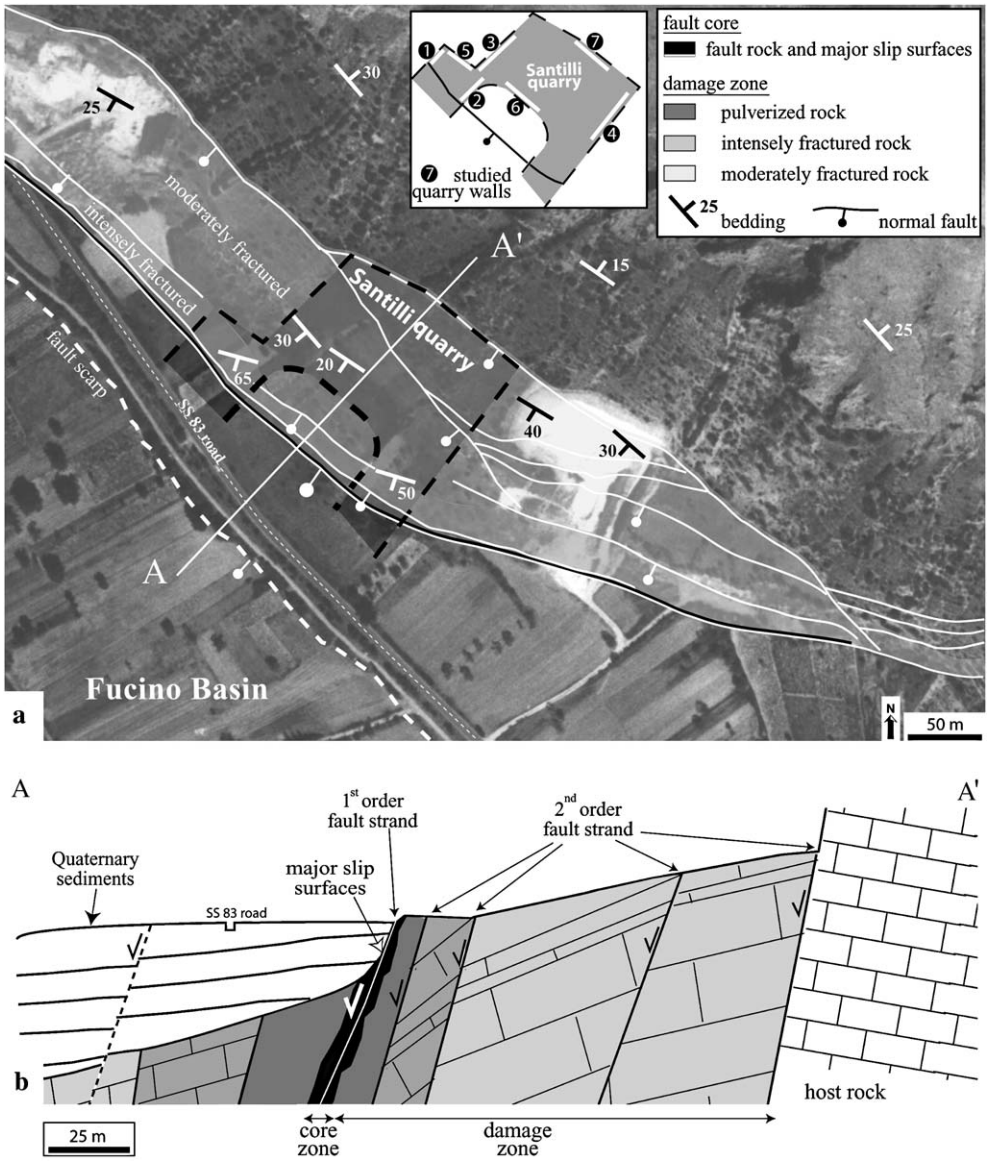

Fig. 3. (a) Aerial distribution of the structural domains in the footwall of the south-central portion of the Venere fault zone (see Fig. 2 for location). The trace of the first-order fault strand (black and white double line) and second-order fault strand (white line) is also shown; the former is characterized by an offset of a few hundred meters, the latter of a several tens of meters. The locations of seven vertical walls studied in the Santilli Quarry (#1 to 7) are shown in the inset. (b) Simplified geological section A–A′ across the Venere fault zone (see Fig. 3a for location, with first-order and second-order fault strands identified). In this section we show an asymmetrical distribution of the fault domains across the fault core. Since the extent of the fault zone in the hanging wall is generally greater than in the footwall (Berg and Skar, 2005 and references therein), we assume that both intensely fractured and pulverized domains of the Venere hanging wall buried underneath the continental basins are about 2 times thicker than those of the footwall.

part of the core of the first-order strand, are covered by the Quaternary sediments (Fig. 3b).

The fault core of the first-order fault strand, which forms the core of the Venere fault zone, is composed of both matrix- and cement-supported fault rocks with polished and striated slip surfaces (Fig. 4). These slip surfaces define a strike range of N100–150E (resulting in a northwesterly trend), and a dip range of 40° to 65° S. The striations and orientations of the slickenfibers, where present, are consistent with a predominantly normal slip, with minor left- or right-lateral slip components, depending on the local orientations of the surfaces. The lateral components of slip are more common along the surfaces oriented N100–110E (dextral) and N140–150E (sinistral). Agosta et al (in press) defined the physical and hydraulic properties of rock samples taken from several different fault zones along the southeastern side of the Fucino Basin.

The fault rocks are made up of a stiff pore frame, which means they contain sub-spherical pores, and are characterized by low porosity and low permeability values. Matrix-supported fault rocks (uncemented fault rocks) are comprised of angular to sub-rounded survivor clasts of calcite and rare dolomite, embedded in a fine calcite matrix (Fig. 4b). The size of these clasts generally decreases nearer the slip surfaces of the fault core. At microscale, pressure solution seams and rare veins crosscut the

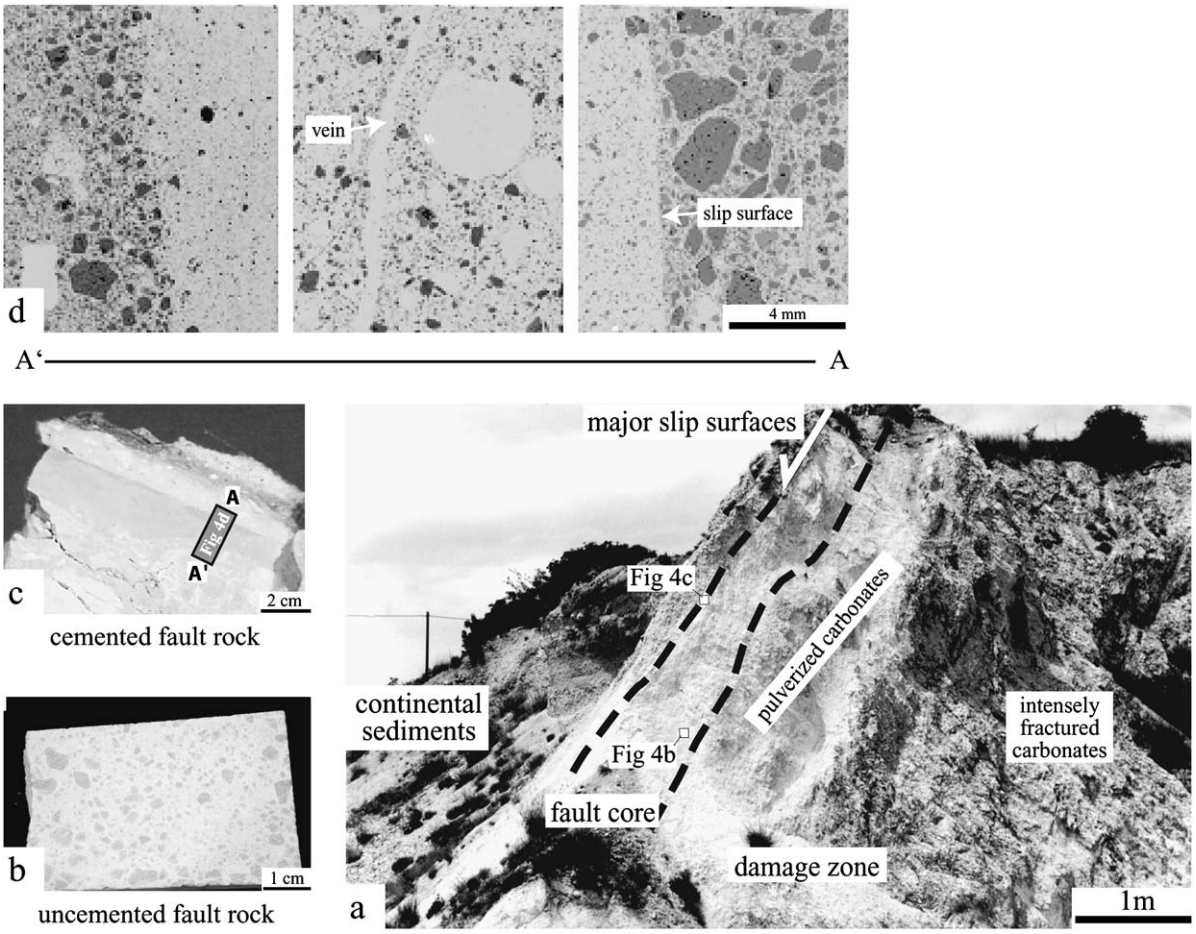

Fig. 4. (a) Cross-sectional view of the fault core of the Venere fault zone juxtaposing the continental sediments of the hanging wall against the deformed carbonates of the footwall. The fault core consists of major slip surfaces and both matrix- and cement-supported fault rocks that are referred as (b) uncemented and (c) cemented fault rocks, respectively. The locations of the two hand-samples shown in b and c are marked in a. (d) Photomicrographs of three thin-sections of the cemented fault rock under polarized light, the location of which is shown in c. The cemented fault rock is made up of survivor clasts with sub-rounded shape embedded in calcite cement and fine-grained matrix, and crosscut by veins that are oriented sub-parallel to the slip surfaces.

matrix-supported fault rock without forming any significant textural anisotropy with respect to seismic velocities. Consequently, these structures do not show any preferential orientation. Cement-supported fault rocks (cemented fault rocks) form a ~1 cm thick zone localized along the major slip surfaces of the fault core. These cemented rocks are made up of subrounded survivor clasts of calcite and rare dolomite, embedded in low-Mg calcite cements and some fine-grained calcite matrix (Fig. 4c). The low-Mg calcite cements precipitated either within micro veins (cf. Fig. 4d) or as meniscus cement from meteoric fluids that mixed with the local groundwater and/or soil before entering the faults (Ghisetti et al., 2001; Agosta and Kirschner, 2003). The micro veins within cemented fault rocks occur mainly sub-parallel to the slip surfaces of the fault core (Fig. 4d), and form a distinctive textural anisotropy relative to seismic velocities.

4.2. Damage zone

The exposed damage zone of the Venere fault zone is characterized by a higher intensity of deformation relative to the Mesozoic platform carbonate host rocks outside of the fault zone. The prominent structural features of the damage zone are the second-order fault strands, which bound slivers of platform carbonate rocks having different deformation intensity and dip angles (Fig. 3a and b). The average thickness of these slivers ranges from 2 to 60 m. The second-order fault strands are sub-parallel to the first-order strand, dip towards the SW, and are on the order of a few to several hundred meters long in the south-central part of the Venere fault zone. We identified four second-order fault strands along the section A–A′ (Fig. 3a), which are either entirely confined within the platform carbonates or form a boundary with the Quaternary terraces that are sometimes present on the downthrown sides of the faults (Fig. 3b). These second-order faults are comprised of cemented and uncemented protoclasts (sensu Sibson, 1977) several centimeters thick, and a damage zone a few meters thick. The extent of the damage zone associated to these second-order fault strands is difficult to map, due to the fragmented nature of the surrounding carbonate rocks. Based on this structural development, we estimate a throw on the order of several tens of meters across each of these faults. Striated slip surfaces observed within the second-order fault strands

show predominantly normal slip with minor lateral components, similar to those of the first-order strand.

The third-order faults are those found within the slivers bounded by the second-order faults. These faults, which are characterized by an offset range on the order of a few centimeters to several meters, were mapped along the nearly orthogonal walls of the Santilli Quarry. The quarry's walls are numbered from 1 to 4 (perpendicular to the first-order fault strand, Fig. 5a–d), and from 5 to 7 (parallel to the first-order fault strand, Fig. 6a–c). The third-order faults have undulating geometry, strike sub-parallel to the first- and second-order fault strands, and dip primarily both southwesterly, towards the basin (synthetic), and northeasterly, towards the Serrone Mountain (antithetic). The internal structure of the third-order faults is made up of fragmented and brecciated carbonate rocks and, sporadically, millimeters to centimeters thick comminuted fault rocks. Many different types of fractures are present within the blocks of carbonates bounded by the third-order fault strands. The nature, distribution, crosscutting and abutting relationships of these fractures will be later described in detail.

Except for few isolated, less-deformed, platform carbonate bodies, the damage zone is deformed to such a degree that the rock it contains may be classified as highly fractured and fragmented, although the bedding is still discernible. The degree of deformation intensity within the damage zone of the fault footwall generally increases towards the fault core. Based on this trend, as measured by fracture spacing and grain-size distribution, three domains can be distinguished: (i) pulverized, nearest the fault core, (ii) intensely fractured, and (iii) moderately fractured platform carbonates, farthest from the fault core. Each of these individual domains has a different thickness and lateral distribution (Fig. 3a and b), and shows the original sedimentary features (e.g., bedding) of the Mesozoic carbonates. In the most deformed domain, bedding is preserved within blocks surrounded by fine-grained, pulverized carbonates.

We performed two sets of scanlines along the outcrops #2 and #3 (see inset of Fig. 3a) of the moderately fractured platform carbonate domain outcropping in the Santilli Quarry. Both sets are comprised of two 5 m long horizontal scanlines oriented E–W and N–S, respectively, and one vertical scanline about 2 m long. The data of these two sets of measurements, which represents all fractures (i.e., pressure solution seams, joints, veins, and sheared elements) present along each scanline, are shown in Fig. 7a (outcrop #2) and Fig. 7b (#3). The mean spacing along the two vertical scanlines varies between 5.6 and 10 mm, the mode is between 5.0 and 8.0 mm. The mean spacing along the four horizontal scanlines (two oriented N–S and two E–W) varies between 7.8 and 10.6 mm, the mode ranges between 5.0 and 16.0 mm.

In order to quantify the deformation intensity of both pulverized and intensely fractured carbonates domains, we analyzed the grain size distribution of representative samples collected 2 m (sample 10, pulverized domain, outcrop #1), 5 m (sample 20, intensely fractured domain, outcrop #1), and 10 m (sample 30, intensely fractured domain, outcrop #2) away from the slip surfaces of the fault core. These two domains of the damage zone are characterized by highly fragmented rocks that contain blocks of less-deformed carbonate rocks several centimeters wide. Collecting the samples, we tried to avoid these less-deformed blocks of carbonates. The numbers of equivalent spherical grains of samples 10, 20, and 30, shown respectively in Fig. 7c, d, and e, were plotted against the corresponding class size on log-log graphs (Billi, 2005). The data follow linear trends in the 0.063–8 mm size ranges, indicating a fractal distribution; the best-fit line was calculated using the following power-law relationship:

$$N(S) = S^{-D} \tag{1}$$

where $N(S)$ is the number of particles less than size S, and D is the fractal number, determined by the slope of the best-fit line (Blenkinsop, 1991).

The results of our analyses indicate that sample 10 is characterized by a D number of 2.95, sample 20 of 2.29, and sample 30 of 2.23. These D values correlate well with the ratios between the weights of grains smaller than 0.063 mm ($W_{<0.063}$) and the total weights of the samples (W_{tot}). For $D = 2.95$ (sample 10) the $W_{<0.063}/W_{tot}$ percentage is 6.92%, whereas for $D = 2.23$ and 2.2 (samples 20 and 30) $W_{<0.063}/W_{tot}$ varies between 1.07% and 1.25%, respectively. The D numbers appear therefore to decrease proportionally to the distance from the slip surfaces of the fault core, reflecting the degree of fragmentation of the platform carbonates within the damage zone.

5. Fundamental fracture modes

Fractures are discontinuities in rocks formed by two parallel surfaces that meet at a fracture front, where the relative displacement of originally adjacent points across the surfaces is small relative to fractures length (Pollard and Aydin, 1988 and references therein). Based on the orientation of the displacement vector relative to the fracture front, fractures are classified as mode I (opening mode), mode II (sliding mode), mode III (tearing mode), and anti-mode I (closing mode). Studying the fractures present in platform carbonates, both outside and within the Venere damage zone, we considered both sliding and tearing mode fractures as shearing fractures because the orientation of the propagation front was unknown for most cases. We focused on the mode, pattern, crosscutting and abutting relationships of all fundamental fractures modes to distinguish three different structural assemblages made up of elements that formed during a specific deformation event: (i) overburden of the Mesozoic platform carbonates, (ii) thrust tectonics due to Oligocene–Pliocene contraction of the Apenninic fold and thrust belt, and (iii) extensional tectonics due to Late Pliocene–Early Pleistocene to present day normal faulting. The first two assemblages form the background structures of the Mesozoic platform carbonates, the elements assigned to the third assemblage characterize later deformation due to the activity of the Venere fault.

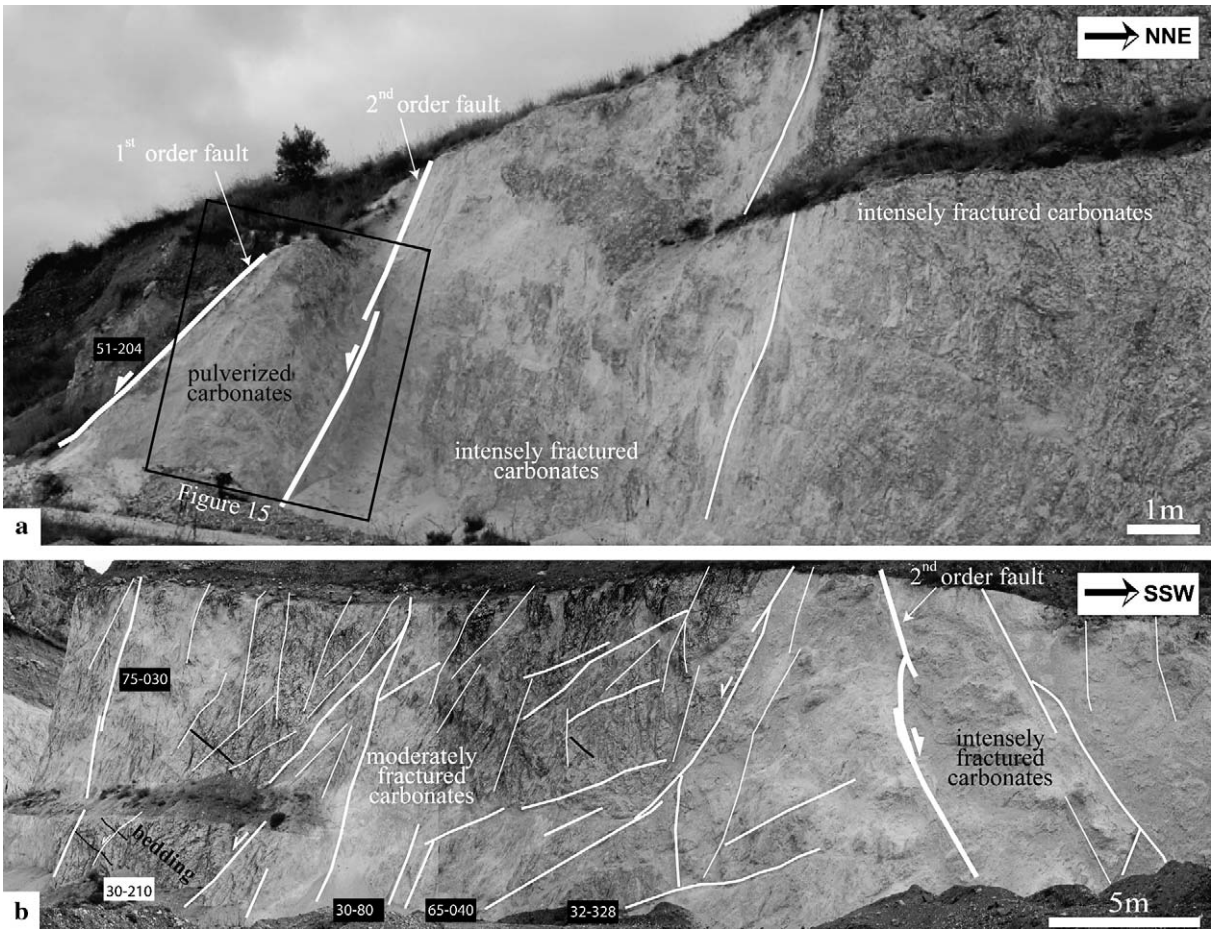

Fig. 5. Sections of the nearly vertical walls of the Santilli Quarry that are oriented orthogonal to the first-order fault strand. The trace of the second fault strands (white thick mark), and third order fault strands with more than 5 cm offset (white mark) are shown. The bedding is denoted with a black mark. (a) Outcrop #1, (b) outcrop #2, (c) outcrop #3, (d) outcrop #4.

5.1. Background elements of Mesozoic platform carbonates

Inspection of the structural elements present in the Mesozoic platform carbonates revealed four sets of pervasive pressure solution seams (Fig. 8). These elements consist of one set of bed-parallel pressure solution seams, labeled PS1, two sets of orthogonal, bed-perpendicular pressure solutions seams, PS2a and PS2b, and one set of pressure solution seams oblique to bedding, PS3. The bed-parallel PS1 seams have columnar form, spacing on the order of a few centimeters to tens of centimeters, length of several meters, and show evidence of shear. These bed-parallel seams determine the mechanical layering of the otherwise massive platform carbonates. The two bed-perpendicular sets, PS2a and PS2b, are confined within the PS1-bounded mechanical layers. Sets PS2a and PS2b have both columnar and wavy forms, centimeter spacing, commonly contain millimeters-thick clayish residue material, and do not show any evidence of shear. Sets PS2a and PS2b strike mainly WNW and ENE, respectively, but their orientations vary within the relay ramp area, dependent on the attitude of the bedding. The PS3 elements are up to several centimeters long and comprised of millimeters-thick clayish residue material. This oblique seams abut both bed-parallel and bed-normal sets, but mainly localize at the tips of the sheared PS1 elements. Bed-parallel, bed-perpendicular, and oblique joints and veins are rare in the Mesozoic carbonate host rocks found outside of the fault zones. On the contrary, both joints and veins occur locally within the Venere fault zone, as it will be documented below.

5.2. Structural elements in the damage zone of the Venere Fault Zone

We first present the structural elements of the moderately and intensely fractured carbonates domains: pressure solution seams and sheared pressure solution seams (PS), and joints, veins, and sheared joints/veins (JV). Then, we assess their role in the evolution of faults with offset ranging from a few centimeters to several tens of centimeters, and document the cataclastic shear bands (CSB) present in the pulverized carbonates domain.

5.2.1. Pressure solution seams (PS)

Based on both orientation, with respect to bedding, and crosscutting/abutting relationships, we identified three more sets of pressure solution seams, PS4a, PS4b, and PS5, in addition to the four sets described above (cf. Fig. 8). These three

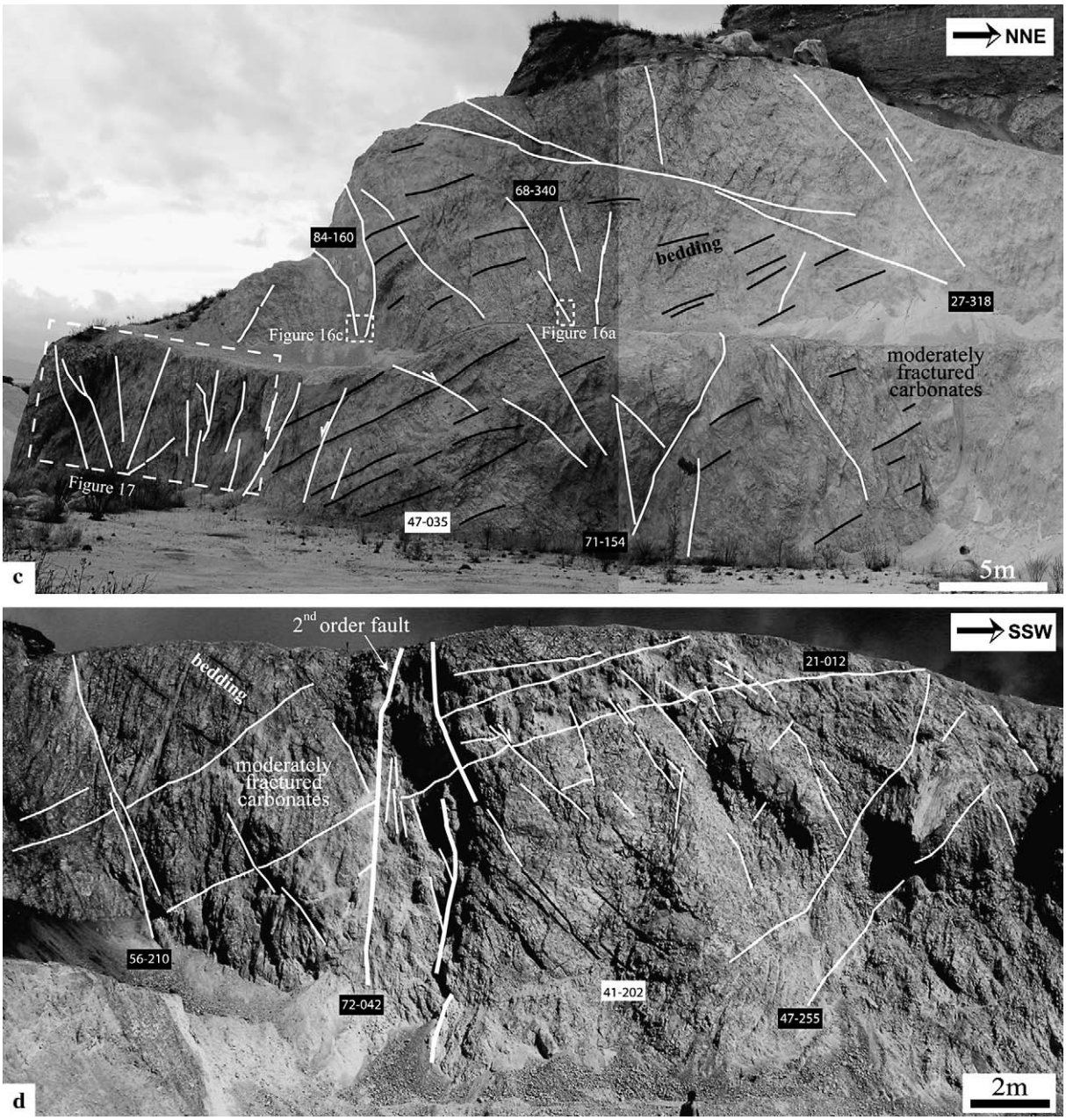

Fig. 5 (*continued*)

sets are all oblique to the bedding and related to sheared pre-existing structural elements. The length, thickness, spacing, down-plunge direction, dip-angle, and shape of all sets of seams present within the Venere fault footwall are listed in Table 1. Some of these properties, such as orientation, are also shown in the supporting maps.

The bed-parallel pressure solution seams, PS1, are pervasive in the damage zone and are the first structural elements that formed in the carbonates; all the other elements that are not parallel to bedding truncate against PS1 (Fig. 9) unless they are sheared (e.g., Fig. 10). Often, the PS1 are themselves sheared, showing apparent normal offset within the fault zone (Figs. 9 and 10). Sets PS2a and PS2b are both oriented bed-perpendicular, crosscut each other (Fig. 11), and abut PS1 (see, for example, PS2a in Fig. 9). These bed-perpendicular sets are commonly sheared, showing apparent reverse offset (see, for example, PS2a, Fig. 10) and apparent normal-sinistral offset (PS2b, Fig. 11). The PS3 elements are localized around the contractional quadrants and geometric complexities of sheared PS1 bed-parallel seams (Fig. 9). The PS4a and PS4b sets are concentrated at the tips of, and abut, the sheared elements PS2a (Figs. 10 and 12) and PS2b (Fig. 11), respectively. The PS5 set localizes at the contractional quadrants of the sheared PS4a set, which shows apparent reverse offset (Fig. 12).

5.2.2. Joints and veins (JV)

Based on crosscutting and abutting relationships, we identified seven sets of opening mode fractures, labeled JV1, JV2a,

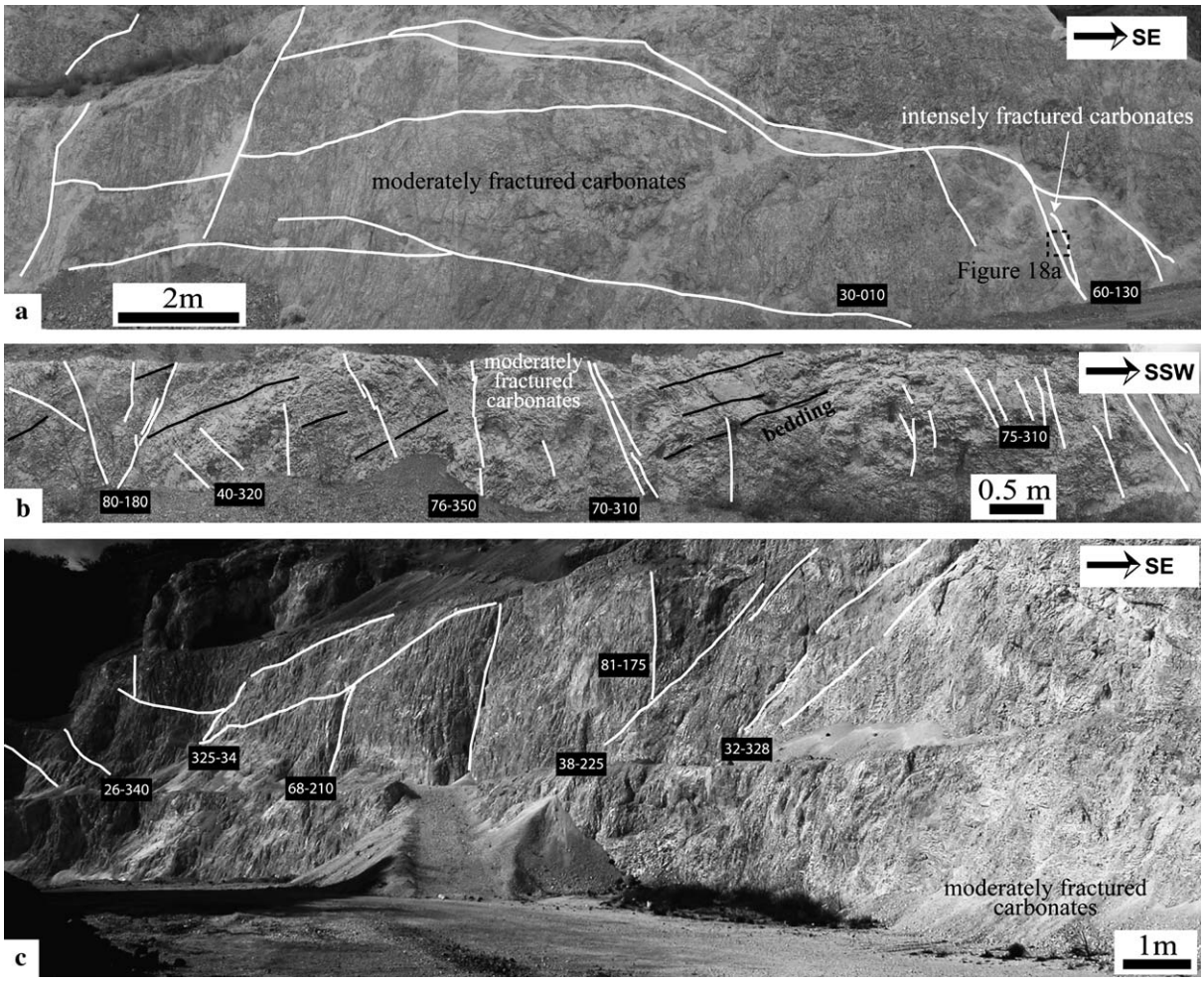

Fig. 6. Sections of the nearly vertical walls of the Santilli Quarry that are oriented parallel to the first-order fault strand. The trace of the third order fault strands with more than 5 cm offset is shown with a white mark, the bedding is denoted with a black mark. (a) Outcrop #5, (b) outcrop #6, (c) outcrop #7.

JV2b, JV3a, JV3b, JV4, and JV5. The veins are filled with calcite and/or chlorite, while the joints contain no infilling material. The length, thickness, spacing, down-plunge direction, dip-angle, and infilling material of each of these sets are reported in Table 2.

The oldest opening mode fractures are the bed-parallel veins JV1, which are present only at few outcrops in the study area (Figs. 9 and 10). Two sets of bed-perpendicular veins, JV2a and JV2b, crosscut each other and are confined within the PS1-bounded mechanical layers (Figs. 9 and 10). Sets JV2a and JV2b have mutually crosscutting relationships with PS2a and PS2b (e.g., JV2a and PS2b in Fig. 11); both show apparent normal offset (Figs. 13 and 14). The remaining four sets of joints and veins (JV3a, JV3b, JV4, and JV5) are oriented oblique to the bedding. The joints and veins JV3a and JV3b are localized around the tips of, and terminate against, the two bed-perpendicular sets, JV2a (Fig. 13) and JV2b (Fig. 14), respectively. The JV4 elements abut against, and are localized at the tips of, the sheared PS1 seams (Figs. 9 and 13). Additional sets of joints that formed after the JV3a, JV3b, and JV4 sets are present within the damage zone. However, these joints are difficult to identify due to their short lengths, lack of infilling material, and obliteration by fragmentation. JV5 is one such later set identifiable within the pulverized carbonate rocks (Fig. 15).

5.2.3. Transition from the fundamental elements to faults

The aforementioned fundamental elements play an important role in the development of faults with offsets of a few centimeters to several meters in the damage zone. The internal architecture of a fault with an offset of about 5 cm (Fig. 16a) is made up of short, PS1-bounded, slip surfaces that parallel primarily the JV2a and PS2a elements and border isolated pods of fragmented rocks (Fig. 16b). The architecture of a nearby fault with more than 20 cm offset (Fig. 16c) is shown in the detailed map of Fig. 16d. This fault is made up of two throughgoing slip surfaces, which cut across many mechanical layers and bound a zone of fragmented and brecciated rocks several centimeters wide.

Two sets of faults with larger displacements, on the order of several tens of centimeters, are identified, one synthetic and one antithetic to the fault core of the first-order fault strand (Fig. 17a–c). The abutting and crosscutting relationships of these two sets of faults to the surrounding structural elements

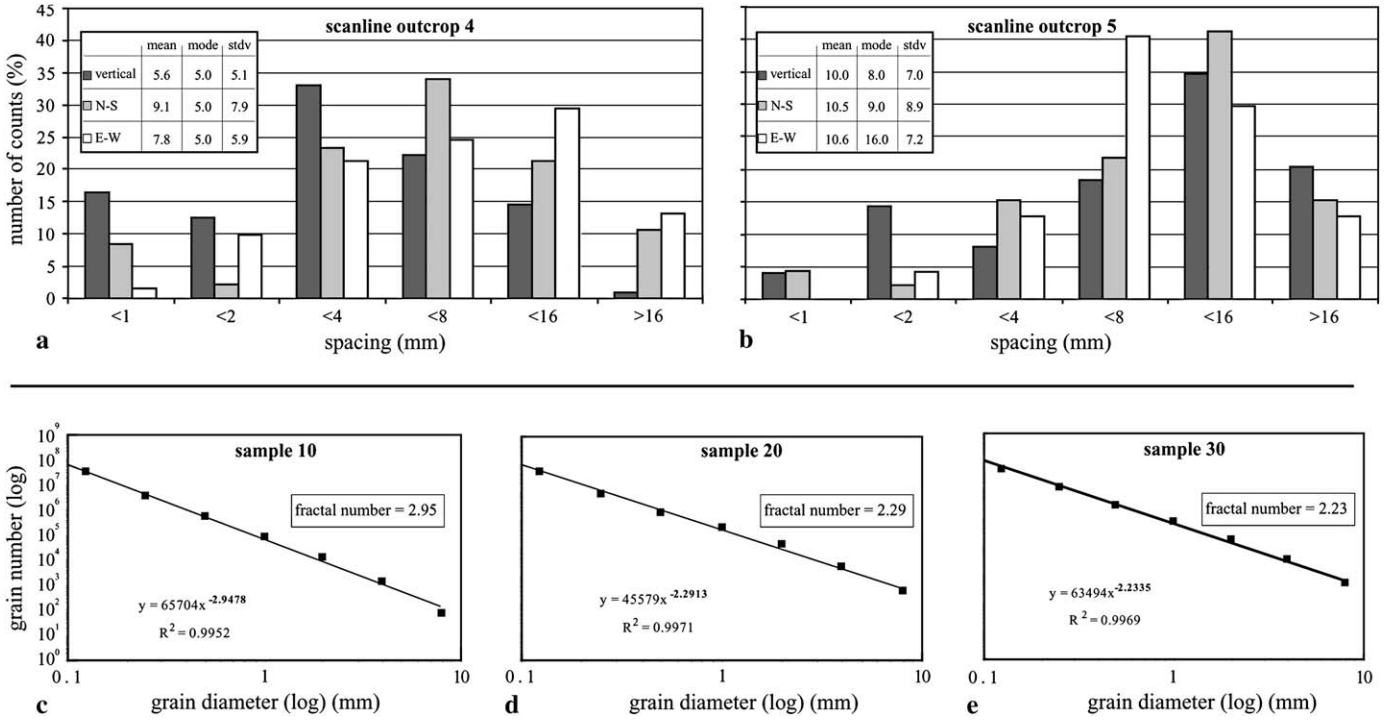

Fig. 7. (a, b) Frequency of fracture spacing for the two sets of scanlines carried out along the outcrops #4 and 5 of the Santilli quarry. Each set consists of three orthogonal scanlines: vertical (2 m long), N–S (5 m long) and E–W (5 m long) oriented, respectively. The mean, mode, and standard deviation of the spacing for each scanline data are shown, in millimeters, in the insets. (c–e) Log–log graphs showing the relationship between frequency-grain size for pulverized and intensely fractured platform carbonates samples collected along the outcrops #1 (samples 10 and 20) and #2 (sample 30) of the Santilli Quarry. The solid lines are the relative power-law best fit.

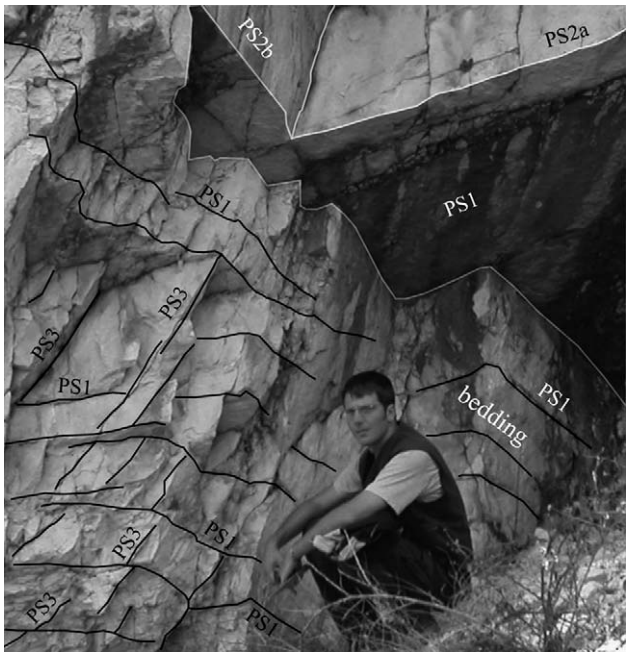

Fig. 8. Background deformation of the Mesozoic platform carbonates outside of the major normal fault zones at the Santuario di Venere (full name: Santuario Madonna del Buon Consiglio, Venere town), whose location is shown in Fig. 2. This deformation consists of four sets of pressure solution seams. One set is bed-parallel, PS1, two are bed-perpendicular, PS2a and PS2b, and one is oblique to bedding, PS3. The PS1 are the oldest elements against which both PS2a and PS2b abut. The oblique PS3 set also terminate against the bed-parallel seams, consistent with their formation due to shearing, with reverse sense, of the PS1 seams.

are consistent with the hierarchical formation of tail joints, as well as the dilation of pre-existing elements, at the extensional quadrants of sheared parent structures. This relationship between slip surfaces and tail joints is no longer visible in the intensely fractured carbonates. In this domain of the damage zone, the slip surfaces show reddish alteration, bound millimeters to centimeters thick, fine-grained, comminuted fault rocks, and are surrounded by highly fragmented carbonate rocks (Fig. 18a and b).

5.2.4. Cataclastic shear bands (CSB)

A system of cataclastic shear bands is present within the pulverized platform carbonates domain of the damage zone in the Santilli Quarry (Fig. 15a and b). These bands are tabular in shape with a thickness of 1 to 15 cm, and show normal offsets. The thicker shear bands are made up of several thinner individual elements that coalesced together. Visual inspection indicates that these tabular bands are comprised of much smaller, fragmented grains than the surrounding pulverized carbonate rocks.

The cataclastic shear bands occur in three major sets of different thicknesses and attitudes (Table 3). The shear bands in set CSB1 are sub-parallel to the slip surfaces of the fault core, and localize at the edges of the pulverized domain. Both density and thickness of the CSB1 bands increase nearer the fault core. The shear band zone adjacent to the fault core merges into the mechanically derived fault rock, forming a continuous transition from the damage zone to the fault rocks of the core. The two other sets (CSB2 and CSB3) are confined between the CSB1 shear bands and are oriented obliquely to the CSB1 elements. Generally, the CSB2 shear bands offset the CSB3 set with normal sense of up to a few centimeters. Both the CSB2 and CSB3 shear bands are normally offset by a few centimeters by the sheared joints JV5.

6. Discussion

The complexity of the platform carbonate rock deformation, involving multiple generations of dissolution and brittle fracturing under various loading conditions, has presented two major challenges to our study. First, the identification of the modes and multiple sets of fundamental structural elements within the Venere fault footwall was difficult due to the highly fragmented nature of the damage zone. Second, the characterization of the tectonic environment in which the various elements formed was problematical. In this regard, we were required to base our interpretation not only on the mode, kinematic, orientation, and abutting relationships documented in the field, but also on the results of previous works done in similar rocks.

6.1. Background deformation

The background elements developed prior to normal faulting during burial diagenesis and thrust tectonics. We consider the overburden assemblage made up of bed-parallel pressure solution seams, PS1, and rare bed-parallel veins, JV1 (Fig. 19a). The PS1 set formed pervasively within the platform

Table 1
Length, thickness, spacing, down-plunge direction, dip-angle, and shape of the different sets of pressure solution seams and sheared pressure solution seams present in the damage zone of the footwall of the Venere fault zone

Set	Length (L)	Thickness (D)	Spacing (S)	Down-plunge direction (a)	Dip-angle (b)	Shape
PS1a	$1 < L < 100$ s	$0.1 < D < 1$	$0.1 < S < 50$	$188 < a < 065$	$20 < b < 65$	Columnar
PS2a	$1 < L < 20$	$0.05 < D < 0.5$	$0.1 < S < 8$	$020 < a < 035$	$15 < b < 45$	Wavy and columnar
PS2b	$1 < L < 10$	$0.05 < D < 0.3$	$0.1 < S < 5$	$250 < a < 265$	$70 < b < 75$	Wavy and columnar
PS3	$0.2 < L < 7$	$D < 0.2$	$S < 2$	$200 < a < 055$	$05 < b < 40$	Wavy, not columnar
PS4a	$L < 5$	$D < 0.1$	$S < 1$	$005 < a < 015$	$60 < b < 75$	Wavy, not columnar
PS4b	$L < 1$	$D < 0.1$	$S < 1$	$235 < a < 240$	$40 < b < 45$	Wavy, not columnar
PS5	$L < 0.5$	$D < 0.1$	$S < 1$	$035 < a < 040$	$38 < b < 41$	Wavy, not columnar

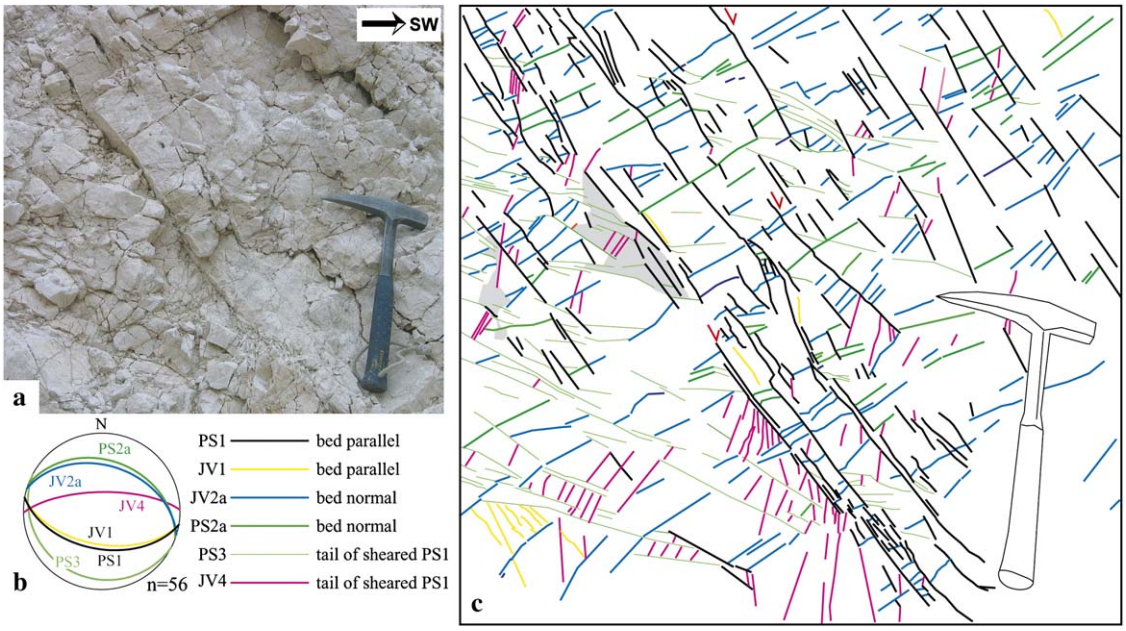

Fig. 9. (a) Photograph of a portion of outcrop #4 (see Fig. 5d for location). (b) Low-hemisphere projection of the structural elements that are presented in c. The hammer is for scale. The oldest structural elements are the bed-parallel pressure solution seams, PS1, which bound the bed-perpendicular veins, JV2, and the pressure solution seams, PS2a. The PS1 with larger trace lengths show apparent normal slip forming tail joints and veins, JV4, and pressure solution seams, PS3. Note that the JV4 set abut against the PS3 seams, indicating that JV4 are the youngest set. Millimeter-thick veins sub-parallel to the bedding, JV1, are also present.

carbonates at overburden pressures probably >25 MPa (>1 km, Ghisetti and Vezzani, 1999) throughout the region, forming mechanical layers whose lengths are much greater than their thicknesses. The small and sporadic veins JV1, which predate all bed-perpendicular and oblique fractures, may also have developed during burial diagenesis. Alternatively, the JV1 set may have formed during early horizontal contraction, perhaps due to high fluid pressures that overcame the vertical loading (Hubbert and Rubey, 1959; Srivastava and Engelder, 1990). The bed-orthogonal veins JV2a, which are confined within the PS1-bounded mechanical layers, may also have developed during burial diagenesis in response to overburden stress and unequal horizontal principal stresses (dashed lines in Fig. 19a).

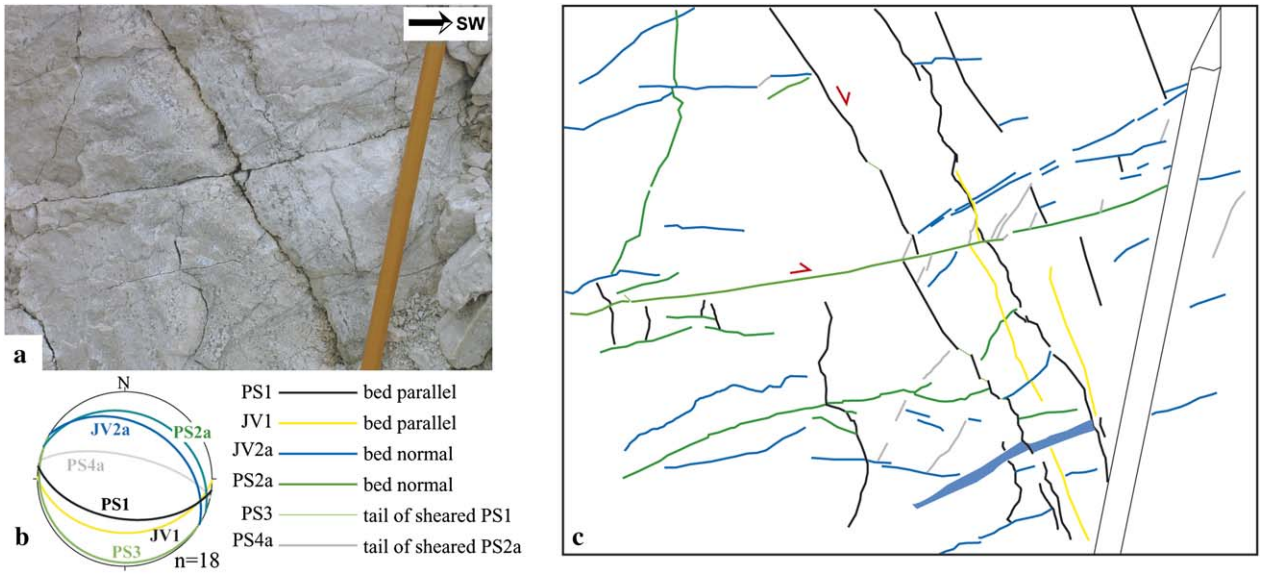

Fig. 10. (a) Photograph of a portion of outcrop #4 (see Fig. 5d for location). (b) Low-hemisphere projection of the structural elements that are reported in c. The pencil is for scale. The sheared bed-parallel pressure solution seams, PS1, offset ~0.3 mm a bed-perpendicular vein, JV2a (thick blue lines), and produced that tail pressure solution seams PS3. Apparent reverse slip of the bed-perpendicular pressure solution, PS2a, offset the PS1 of about 1 cm, and determined the formation of tail pressure solution seams PS4a at their contractional tips. Millimeter-thick veins that sub-parallel the bedding, JV1, are also present.

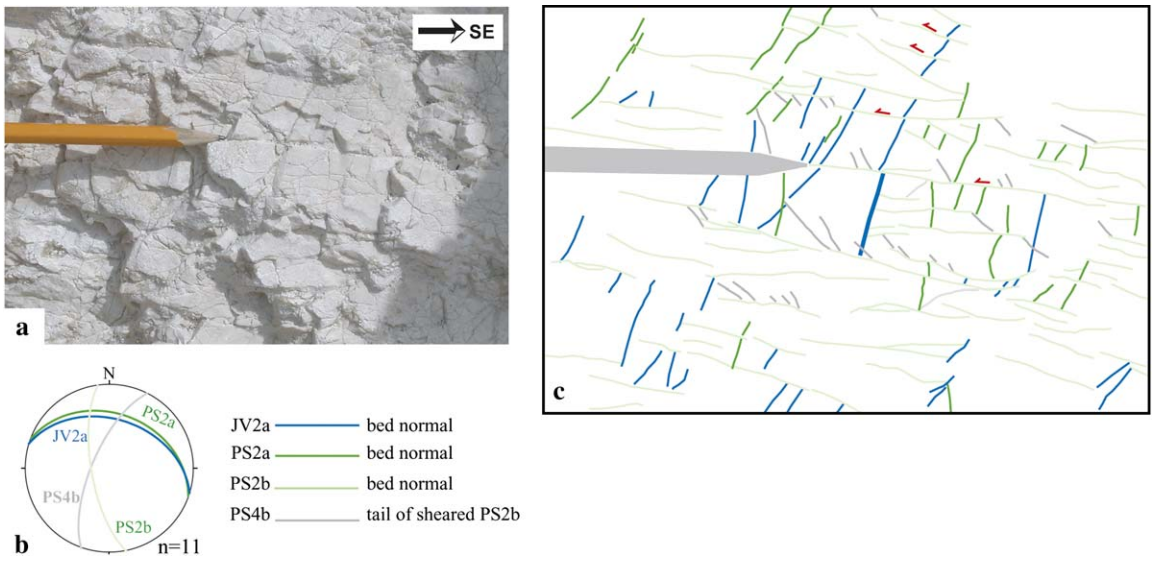

Fig. 11. (a) Photograph of a portion of outcrop #7 (Fig. 6c). (b) Low-hemisphere projection of the structural elements that are reported in c (pencil for scale). Mutual crosscutting relationships are shown between the bed-perpendicular pressure solution seams PS2a and PS2b and between the PS2b set and the bed-perpendicular veins JV2a. Shearing of the PS2b seams produced tail pressure solution seams, PS4b, which localized at the tips and around geometric complexities of the PS2b elements.

The thrust structural assemblage includes the bed-perpendicular elements, PS2a, PS2b, JV2a, and JV2b, which formed during early thrusting when the beds were flat (pre-tilting, Fig. 19b), and the oblique seams PS3 that developed later on when the beds were inclined (syn-tilting, Fig. 19c). Previous works have reported the association between bed-parallel pressure solution seams and bed-perpendicular veins (Nelson, 1981), and between bed-parallel and bed-perpendicular pressure solution seams (Graham et al., 2003, in press). In this study we document mutually abutting relationships between bed-perpendicular pressure solution seams, PS2a and PS2b, and veins, JV2a and JV2b (cf. Fig. 11). A similar paired relationship was previously reported by Arthaud and Mattauer (1970) and Groshong (1988), which indicates that pressure solution seams and joints/veins are, more or less, contemporaneous. However, as noted above, it is possible that some of the JV2a veins might have formed during burial diagenesis.

The mutual abutting relationship between bed-perpendicular seams (resulting from closing mode failures occurring perpendicular to the greatest principal stress, Fletcher and

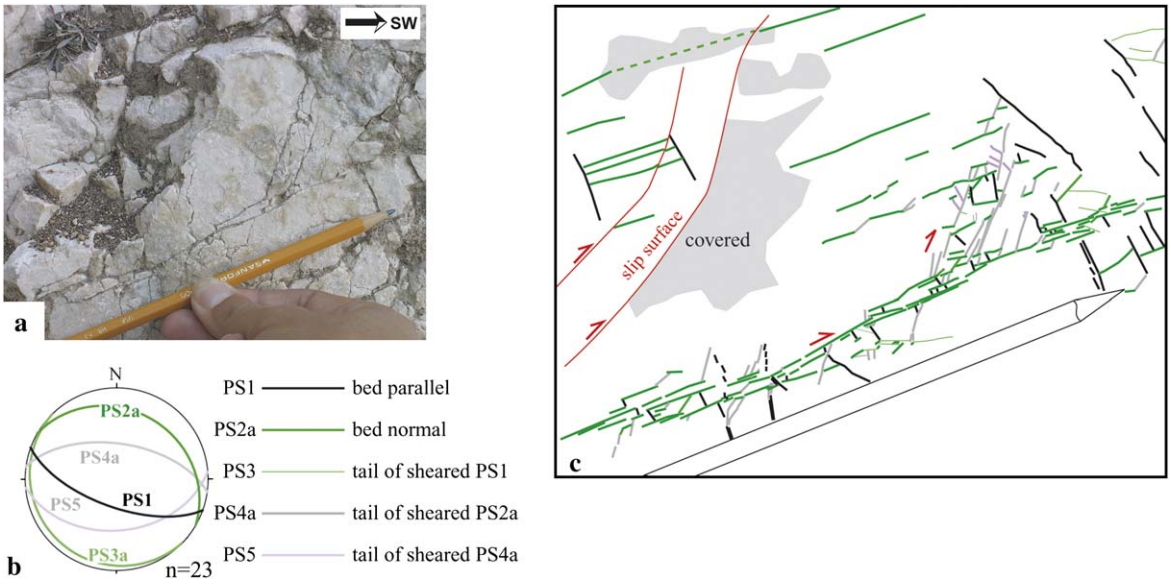

Fig. 12. (a) Photograph of a portion of outcrop #2 (see Fig. 5b for location). (b) Low-hemisphere projection of the structural elements that are presented in c. The pencil is for scale. Shearing of the bed-perpendicular pressure solution seams PS2a with apparent reverse sense produced the tail pressure solution seams PS4a. The PS4a set, which localize at the contractional tips, and around geometric complexities, of the sheared PS2a elements, was in turn sheared with apparent reverse sense to form a new set of tail pressure solution seams, PS5.

Table 2
Length, thickness, spacing, down-plunge direction, dip-angle, and infilling of the different sets of joints and veins and sheared joints/veins present in the in the damage zone of the footwall of the Venere fault zone

Set	Length (L)	Thickness (D)	Spacing (S)	Down-plunge direction (a)	Dip-angle (b)	Infilling (when present)
JV1	$3 < L < 10$	$0.1 < D < 0.7$	$0.1 < S < 10$	$190 < a < 210$	$30 < b < 45$	Calcite
JV2a	$0.5 < L < 9$	$0.01 < D < 0.6$	$0.1 < S < 8$	$015 < a < 035$	$35 < b < 45$	Calcite and chlorite
JV2b	$0.2 < L < 11$	$0.01 < D < 0.3$	$0.1 < S < 5$	$260 < a < 315$	$65 < b < 80$	Calcite and chlorite
JV3a	$L < 4$	$D < 0.05$	$S < 0.5$	$050 < a < 060$	$60 < b < 70$	Calcite
JV3b	$L < 5$	$D < 0.03$	$S < 0.5$	$125 < a < 130$	$60 < b < 65$	Calcite
JV4	$0.1 < L < 12$	$D < 0.05$	$S < 1$	$190 < a < 350$	$45 < b < 70$	Calcite
JV5	$L < 0.5$	$D < 0.01$	$S < 2$	$030 < a < 040$	$70 < b < 85$	

Pollard, 1981), and joints/veins (resulting from opening mode failures occurring perpendicular to the least principal stress, Pollard and Aydin, 1988), indicate the systematic reversal in the greatest and least principal stresses. In order to explain this switch of the stress axes, we invoke a mechanism of stress relaxation and reloading analogous to that proposed for the formation of orthogonal opening mode fractures by Bai et al (2002). The orthogonal PS2a and JV2b might have developed under a greatest principal stress axis oriented ~E–W and an axis of least principal stress oriented ~N–S; at local scale, the switching of these two axes due to relaxation and reloading was probably responsible for the formation of both PS2b and JV2a sets.

The oblique pressure solution seams of set PS3 abut against both sheared bed-parallel and sheared bed-perpendicular structural elements (Fig. 9). These relationships are consistent with their formation as tail pressure solution seams of pre-existing elements that were subjected to shearing in accordance with the local E–NE transport direction of the thrust sheets (Vezzani and Ghisetti, 1998). The shearing responsible for the oblique pressure solution seams might have been due to progressive rotation of either the carbonate beds or the principal stresses. The conceptual model in Fig. 19c shows the former case. Graham et al (2003) came to a similar conclusion to explain the formation of oblique pressure solution seams in the platform carbonates of the Maiella thrust sheet, in central Italy. The orientation, distribution, and abutting relationships of joints and veins JV4 oblique to the bedding (dashed lines in Fig. 19c) suggest that these opening mode fractures may have also formed during the later stages of thrust tectonics, but only after the PS3 set (cf. the abutting relationship shown in Fig. 9). Another scenario for the formation of the joints and veins JV4, related to normal faulting, will be presented in the next section.

6.2. Deformation due to normal faulting

We propose a conceptual model of normal fault growth in platform carbonate rocks characterized by the deformation background discussed above. This model involves four different stages of deformation that occurred during regional uplift and exhumation from depths of 1 to 2 km. The first stage of

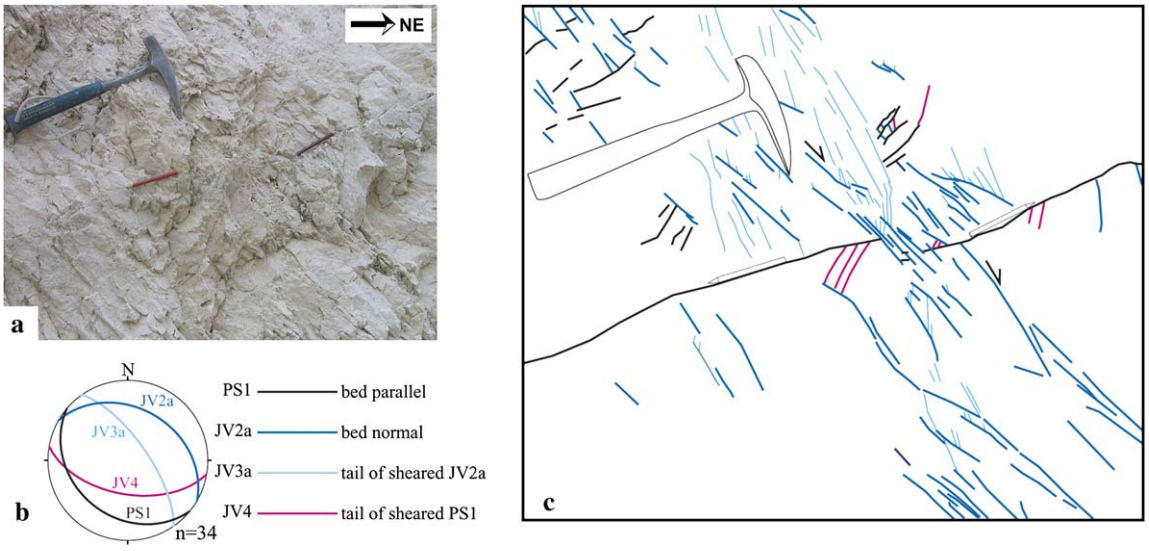

Fig. 13. (a) Photograph of a portion of outcrop #3 (see Fig. 5c for location). (b) Low-hemisphere projection of the structural elements that are reported in c. The hammer is for scale. The top of a dark bed, marked by two pencils, is offset ~2 cm by the bed-perpendicular veins JV2a. Apparent normal slip of the JV2a elements produced tail joints/veins, JV3a, at their extensional quadrants. The tail opening mode fractures JV4 of the normally sheared bed-parallel pressure solution seams, PS1, are also shown in the figure.

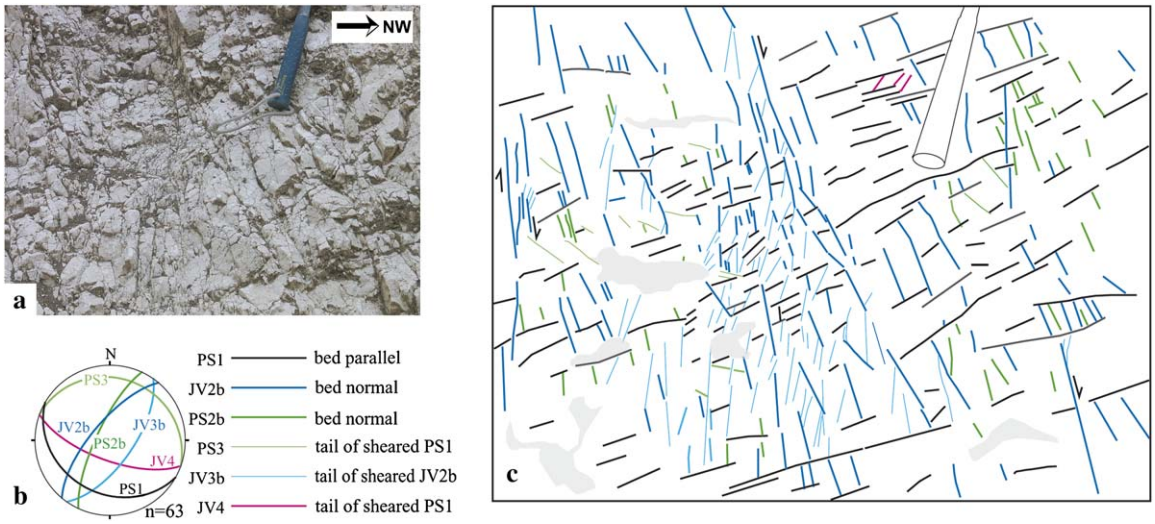

Fig. 14. (a) Photograph of a portion of outcrop #6 (see Fig. 6b for location). (b) Low-hemisphere projection of the structural elements that are presented in c. The hammer is for scale. Shearing along bed-perpendicular veins JV2b with apparent normal sense formed tail joints and veins, JV3b, in their extensional quadrants. The bed-perpendicular, PS2b, and oblique, PS3, pressure solution seams and the oblique joints and veins JV4 are bounded by the bed-parallel pressure solution seams, PS1.

incipient normal faulting (Fig. 20a) took place by shearing of the pre-existing, primarily bed-perpendicular, elements under a vertical greatest principal stress axis, such as that presumed to be the driving force for the extension of CADA (Ghisetti and Vezzani, 1999). This produced tail pressure solution seams in the contractional quadrants (PS4a and PS4b, cf. Figs. 10–12) and joints/veins in the extensional quadrants (JV3a and JV3b, cf. Figs. 13 and 14) of the sheared seams and joints/veins. This relationship between a sheared fracture and the tails fractures has been extensively documented by Rispoli (1981), Ohlmacher and Aydin (1995), Willemse et al (1997), and Kim et al (2004), and modeled by Fletcher and Pollard (1981) and Petit and Mattauer (1995). The coalescence of the oblique, normal fault-related, tail fractures with the pre-existing, bed-perpendicular and oblique elements defined small pods of fragmented rocks within the individual mechanical layers. The resulting architecture of the incipient normal faults was therefore made up of short, discontinuous slip surfaces that

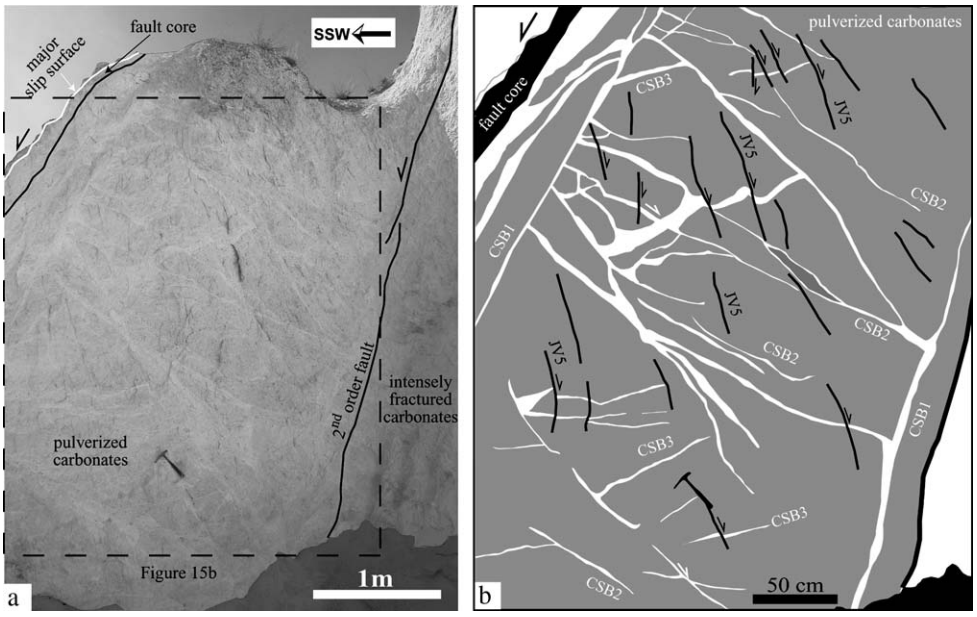

Fig. 15. (a) Photograph of the pulverized carbonates domain that flanks the fault core of the Venere fault zone along outcrop #1 (see Fig. 5a for location). The pulverized domain is bound by the fault core on the hanging wall side and by a second-order fault strand on the footwall side. (b) Close-up of the pulverized domain. Three sets of cataclastic shear bands, CSB1 to CSB3, and one set of joints and sheared joints, JV5, crosscut the pulverized carbonates. The CSB1 set is sub-parallel to the fault core and localizes at the peripheries of the pulverized domain. The CSB2 offset with apparent normal sense the CSB3 set. The JV5 set appears to postdate both CSB2 and CSB3 sets.

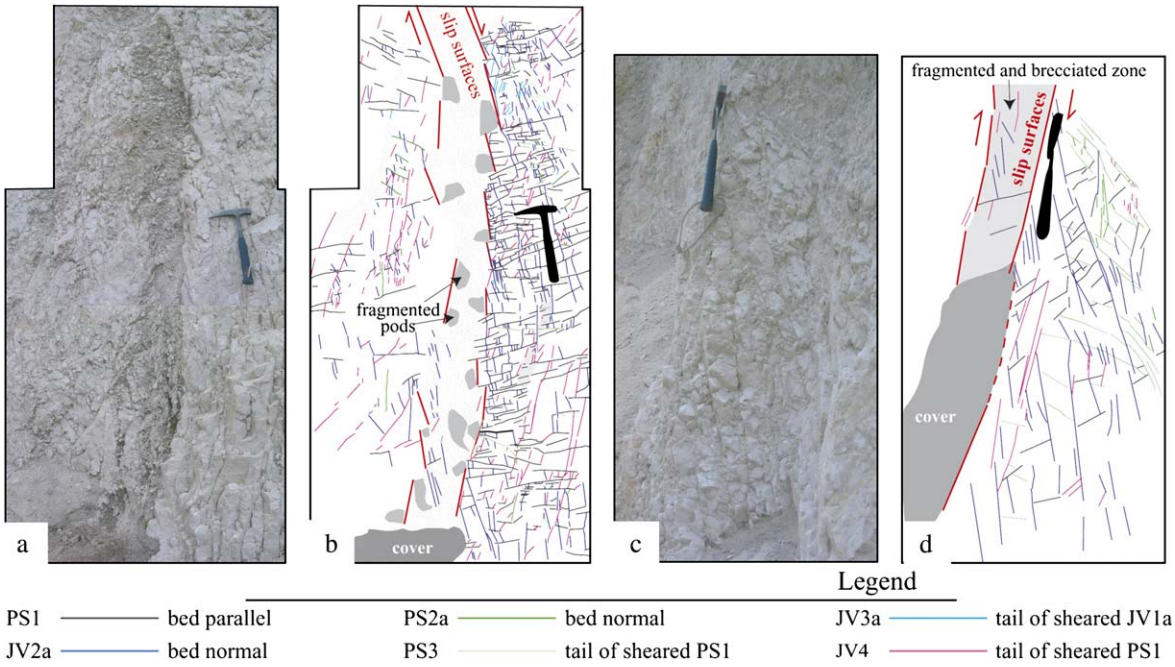

Fig. 16. (a) Photograph of a normal fault with about 5 cm of apparent normal offset marked in Fig. 5c. (b) The fault shown in a consists of discontinuous, strata-bounded, slip surfaces and isolated pods of fragmented carbonates. The slip surfaces formed along the pre-existing JV2a and PS2a elements. (c) Photograph of a normal fault with about 20 cm offset marked in Fig. 5c. (d) The fault shown in c is made up of about 30 cm thick fragmented and brecciated carbonates bounded by throughgoing slip surfaces that cut across the different mechanical layers.

bounded pods of fragmented rocks (cf. Fig. 16b). The offset of these faults was on the order of a few centimeters.

The development of oblique pressure solution seams and/or tail joints/veins marks a new stage of fault development in carbonate rocks, as proposed by Petit and Mattauer (1995), Willemse at al (1997), and Salvini et al (1999) for strike slip faults, and by Graham et al (2003, in press) for normal and thrust faults, respectively. Both closing mode fracturing (a time-dependent, slow process) and opening mode fracturing (a dynamic or quasi-dynamic, brittle process) may have occurred more or less at the same time during incipient faulting. Assuming mass conservation, there are two possibilities to explain the temporal relationships among slip, opening mode fracturing, pressure solution, and possible mineral precipitation. One possibility is that joints opened very slowly, comparable to the rates of rock solubility, so that mass transfer could accommodate slip accumulation, allowing the four mechanisms to occur contemporaneously (fault creep). The second possibility is that opening mode fracturing and slip occurred rapidly (seismic faulting), and the open fractures were later filled during interseismic periods by dissolved carbonate material produced by pressure solution. Based on the available data, neither of these two scenarios can be ruled out.

The second stage of fault growth involved the coalescence of the isolated pods of fragmented rocks across adjacent mechanical beds to form two sets of sub-parallel, NW-striking, throughgoing normal faults (Fig. 20b). One set of normal faults dipped towards the SW (synthetic to the major fault, the first-order fault strand) and one towards the NE (antithetic). We propose that this process occurred by shearing of the favorably oriented, pre-existing elements, and the hierarchical formation and subsequent shearing of both tail pressure solution seams and tail joints/veins. The architecture of the two sets of normal faults was made up of throughgoing slip surfaces that cut across many mechanical layers, and bounded zones of fragmented and brecciated carbonate rocks (cf. Fig. 16d) and, occasionally, fine-grained fault rocks (cf. Fig. 18). The offset of these faults was on the order of a few to several tens of centimeters.

During ongoing deformation and exhumation, the next stage of normal faulting likely occurred after appreciable tilting towards the basin of the normal fault zone due to extension of CADA (Ghisetti and Vezzani, 1999). In our proposed model, this stage was characterized by the growth of the synthetic normal fault set, which commonly have a larger offset relative to the antithetic fault set within the Venere damage zone, and the shearing with normal sense of the bed-parallel PS1 seams (Fig. 20c). Shearing of the PS1 seams produced opening mode tail fractures (JV4, cf. Fig. 9). The orientation of the JV4 set relative to the sheared PS1 seams is also consistent with the kinematics of thrust-related, bed-parallel slip in combination with the tail pressure solution seams PS3 described earlier (cf. Fig. 8). However, based on observations in outcrops outside of the normal fault zone, which do not show tail joints/veins associated with the reversely sheared PS1 seams, we conclude that most of the tail joints and veins JV4 formed during normal faulting. Shearing of the PS1 elements with normal sense appears to be enhanced near the fault core, where the tilting was greater and the angle between bedding and the vertical, greatest principal stress axis smaller.

The fourth and last stage of deformation is thought to be associated with the emergence of the fault zone from depth,

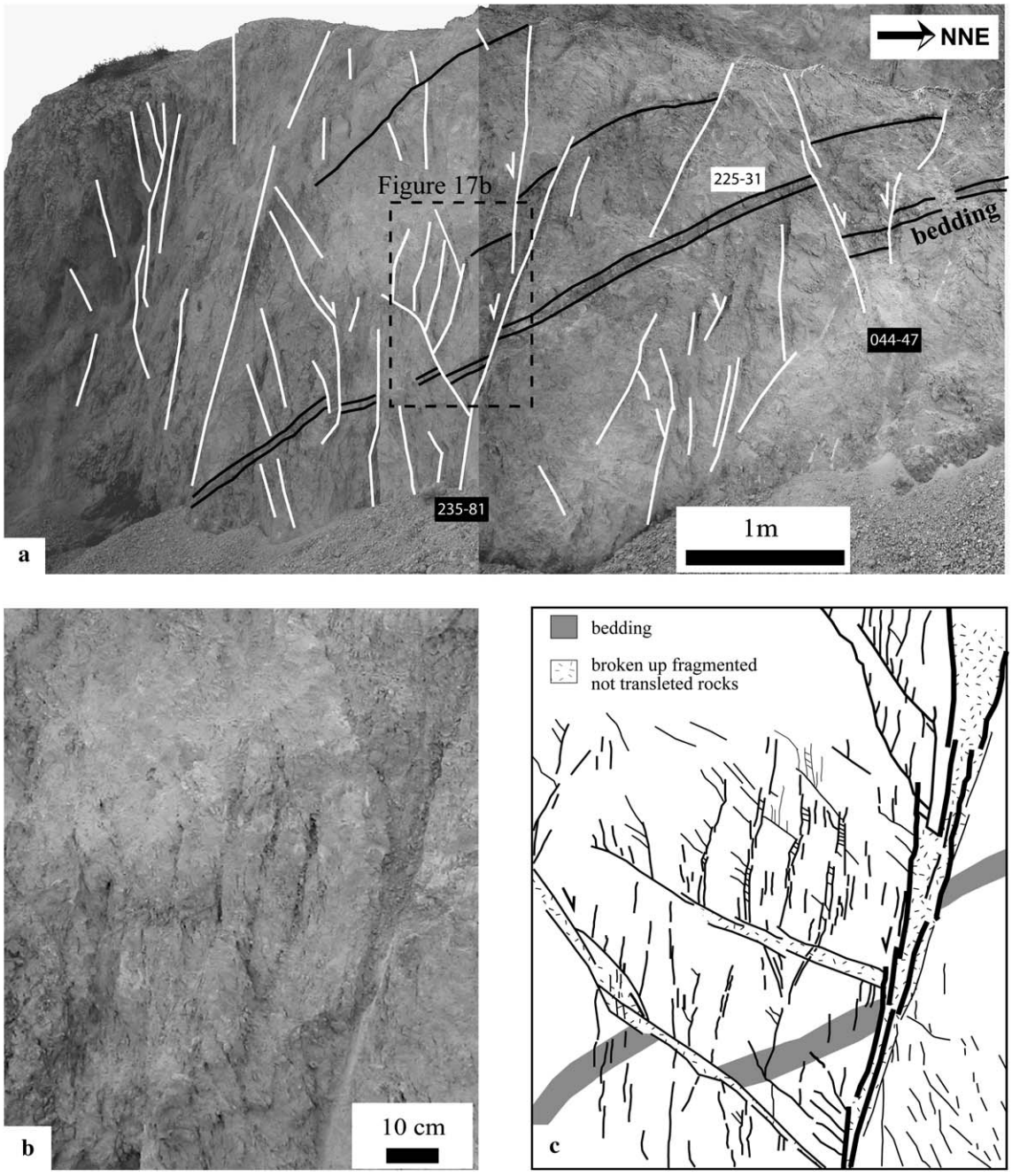

Fig. 17. (a) Close-up of a portion of the vertical wall #3 (see Fig. 5c). The two sets of normal faults characterized by up to several tens of centimeters of apparent throw are synthetic and antithetic to the first-order fault strand, respectively. (b) Close-up of the area marked in a. (c) Map showing the hierarchical formation and shearing of opening mode fractures as well as the dilation and shearing of the pre-existing structural elements.

growth of the basin in the hanging wall, and the juxtaposition of fluvial and lacustrine sediments against the deformed platform carbonates of the footwall (Fig. 20d). The present day fault zone configuration in the footwall is comprised of a fault core up to 1 m thick, and a damage zone up to 100 m thick characterized by higher degrees of deformation nearer the fault core (cf. Fig. 3). This variation in the deformation intensity is well demonstrated by the increasing density of the second-order fault strands, and by the presence of pulverized carbonates adjacent to the fault core. During this last stage of faulting, the pulverized carbonates domain was first deformed by localized cataclastic shear bands, and then by opening mode joints (cf. Fig. 15b). Structures pre-dating these two mechanisms are not apparent and were likely obliterated. Based on this observation, and on the greater number of joints and sheared joints in both pulverized and intensely fractured carbonate domains, we conclude that the latest deformation across the damage zone was accomplished primarily by three main mechanisms: (1) opening mode-based deformation, (2) shearing and dilation of the pre-existing elements (cf.

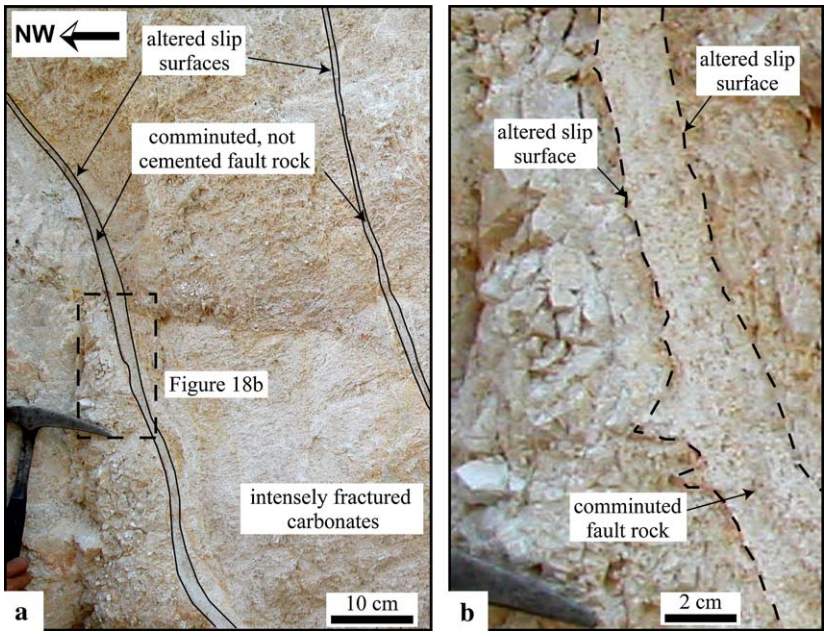

Fig. 18. (a) Close-up of two faults with few tens of centimeters offset that formed within the intensely fractured carbonates domain of the damage zone (see Fig. 6a). (b) Close-up of the faults shown in a (see dashed rectangle). The internal architecture of this fault consists of centimeters-thick comminuted, uncemented fault rocks bounded by throughgoing slip surfaces with reddish alteration.

Fig. 17c), and (3) cataclastic deformation of the pulverized carbonates, as well of the fault rocks of the core. The pressure solution-based deformation mechanism was either absent or minimal within the normal fault zone during this time.

Considering the pulverized carbonates domain, it contains three sets of cataclastic shear bands, CSB1 to CSB3, which are fundamental structural elements characteristic of granular clastic rocks with porosity greater than 15% (Aydin, 1978; Antonellini et al., 1994), and one set of joints and sheared joints, JV5, that postdate both CSB2 and CSB3 sets. The presence of these different structural elements indicates two main changes in the rheology of the platform carbonates during the latest stage of faulting in the most deformed domain if the damage zone. The first change was from a stiff rock, which failed primarily by closing mode fracturing, to a loose, granular rock that failed by shear banding and cataclastic processes. The original low-porosity platform carbonates (Agosta et al., in press) underwent intense deformation at, and adjacent to, the fault core. Adjacent to the fault core, the deformation pulverized the carbonate rock and increased the porosity with respect to that of the undeformed platform carbonate rock. This pulverized material was then undergone strain hardening and loss of the secondary porosity during cataclastic deformation, leading to the formation of new opening mode fractures and their subsequent shearing. A similar change of failure mode in sandstones has been previously described by Davatzes and Aydin (2003) and Aydin et al (2006). The well-developed set of cataclastic shear bands that occurs adjacent and parallel to the fault core, CSB1, merges into the fault rock, which suggests a mechanism responsible for the generation of the fine-grained fault rock in the platform carbonates. It is possible that the fault rocks perpendicular to the fault core grew by incorporating the adjacent cataclastic shear bands (cf. Fig. 15). The addition of fine-grained material into the fault core in the form of organized, discrete, sub-parallel cataclastic shear bands, would be therefore a self-organized process, rather then an abrasion or wearing-based process.

7. Conclusions

The Venere fault has a maximum of 600 m of throw and is made up of deformed basinal sediments in the hanging wall, a fault core (up to 1 m thick) and a damage zone (up to 100 m thick) in the footwall. The footwall is tilted toward the basin relative to the Mesozoic, low-porosity, platform carbonate rocks present outside of the fault zone. The amount of tilting of the fault footwall increases toward the basin. The fault core is comprised of both matrix-supported and cement-supported fault rocks, and first-order slip surfaces that recorded dip-slip and minor strike-slip components. The damage zone of the Venere footwall is crosscut by various second- and third-order faults of differing lengths, spacing, throw, and degrees of deformation. The platform carbonates between

Table 3
Thickness, down-plunge direction, and dip-angle of the three sets of cataclastic shear bands present within the pulverized carbonates domain outcropping along the vertical wall #1 (cf. inset of Fig. 3a) of the Santilli Quarry

Set	Thickness (D)	Down-plunge direction (a)	Dip-angle (b)
CSB1	$D < 15$	$035 < a < 058$	$57 < b < 85$
CSB2	$D < 5$	$015 < a < 041$	$15 < b < 45$
CSB3	$D < 5$	$208 < a < 231$	$31 < b < 65$

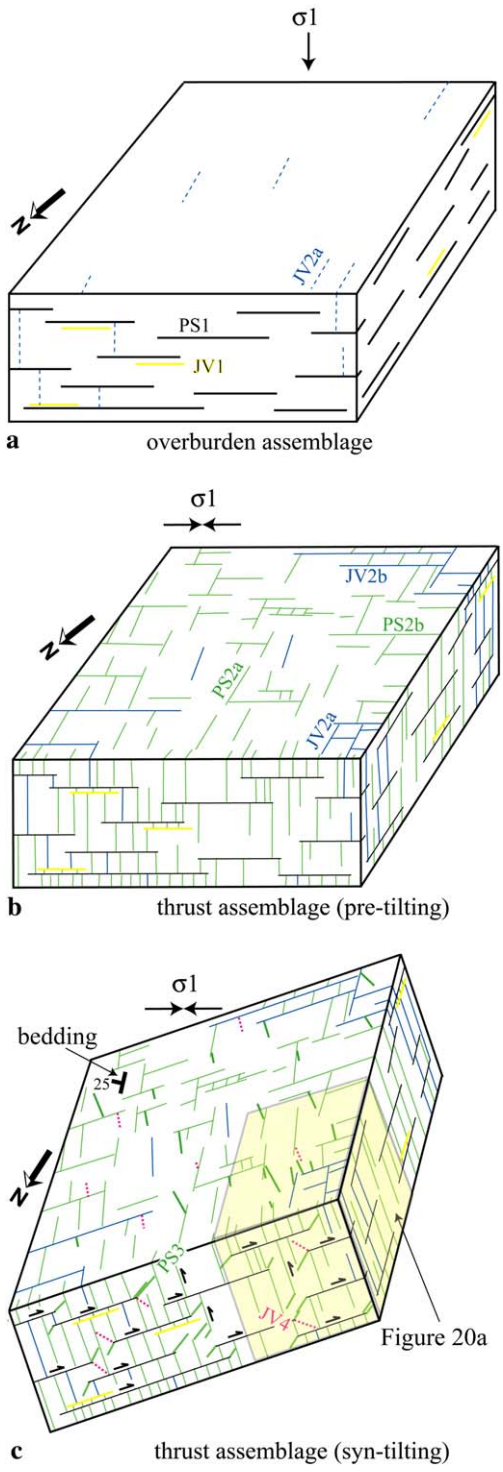

Fig. 19. Idealized block diagrams showing the overburden and thrust structural assemblages that predate normal faulting. The length of the blocks is of a few meters. (a) The overburden assemblage includes bed-parallel pressure solution seams, PS1, and veins, JV1. The bed-perpendicular veins, JV2a, confined within the PS1-bound mechanical layers may also belong to this structural assemblage. (b) The pre-tilting thrust assemblage of the platform carbonates is comprised of two sets of sub-orthogonal pressure solution seams, PS2a and PS2b, and, occasionally, veins, JV2a and JV2b. The direction of the greatest principal stress axis, σ1, reported in the block diagram represents the direction of the maximum compressive regional stress during thrust tectonics inferred from regional geology (after Vezzani and Ghisetti, 1998). (c) Oblique pressure solution seams, PS3, at the tips and around geometric complexities of the sheared PS1 seams mark the rotation and tilting of the mechanical layers. The oblique tail joints and veins JV4 could have also formed during this stage postdating the tail PS3 seams.

adjacent third-order faults are densely crosscut by pressure solution seams, joints/veins, sheared seams, and sheared joints/veins. The frequency of these structures generally increases closer to the fault core. Based on the results of our field observations of the fracture spacing and laboratory analyses of grain size distribution, we distinguished three different domains in the damage zone of the fault footwall: (i) pulverized, (ii) intensely fractured, and (iii) moderately fractured carbonates. The most deformed domain, the pulverized carbonates, flanks the fault core. The three domains of the damage zone are usually bounded by second-order faults. The relative thickness of these domains shows a pronounced lateral variability along the south-central portion of the Venere fault zone.

Normal faulting in platform carbonates initiated by shearing of the pre-existing, primarily bed-perpendicular, structural elements inherited from the earlier thrust tectonics regime. This process produced oblique tail pressure solution seams and joints/veins at the contractional and extensional quadrants of the sheared elements, respectively. Interaction between these new tail fractures and the pre-existing structural elements formed isolated pods of fragmented carbonate rocks within the individual mechanical layers. These isolated pods of fragmented rocks then coalesced across the adjacent mechanical layers to form two sets of conjugate normal faults within the emerging fault zone. With ongoing deformation, exhumation, and tilting of the fault footwall toward the basin, opening and shearing modes deformation became more pronounced within the fault zone relative to closing mode deformation. The last stages of faulting were characterized by the juxtaposition of the basinal sediments of the hanging wall against the deformed carbonates of the footwall. Cataclastic deformation of the fault core and adjacent pulverized carbonates, opening-mode fracturing, as well as shearing and dilation of the pre-existing structural elements of the damage zone were the main processes that occurred during seismic faulting of the Venere fault zone.

Two main rheological and structural changes are tractable in the pulverized carbonates domain of the damage zone: first, the original massive, low-porosity, platform carbonates failed primarily by closing-mode and to a lesser degree by opening-mode fracturing, leading to high fragmentation and pulverization of these rocks. Consequently, the deformed material behaved similar to loose, porous, granular rocks and failed by shear banding and cataclastic processes. Second, this highly comminuted and pulverized carbonates then failed by opening mode fracturing due perhaps to strain hardening by cataclastic deformation. It appears that this is the first time that a double transition in the rheology, from a massive rock to a pulverized high porosity rock, and then to a cohesive, brittle rock has been documented in platform carbonates. The deformation at the fault core/damage zone transition also suggests that the fault rocks of the core grew laterally by a self-organized process that involved the incorporation of the adjacent cataclastic shear bands oriented sub-parallel to the fault core.

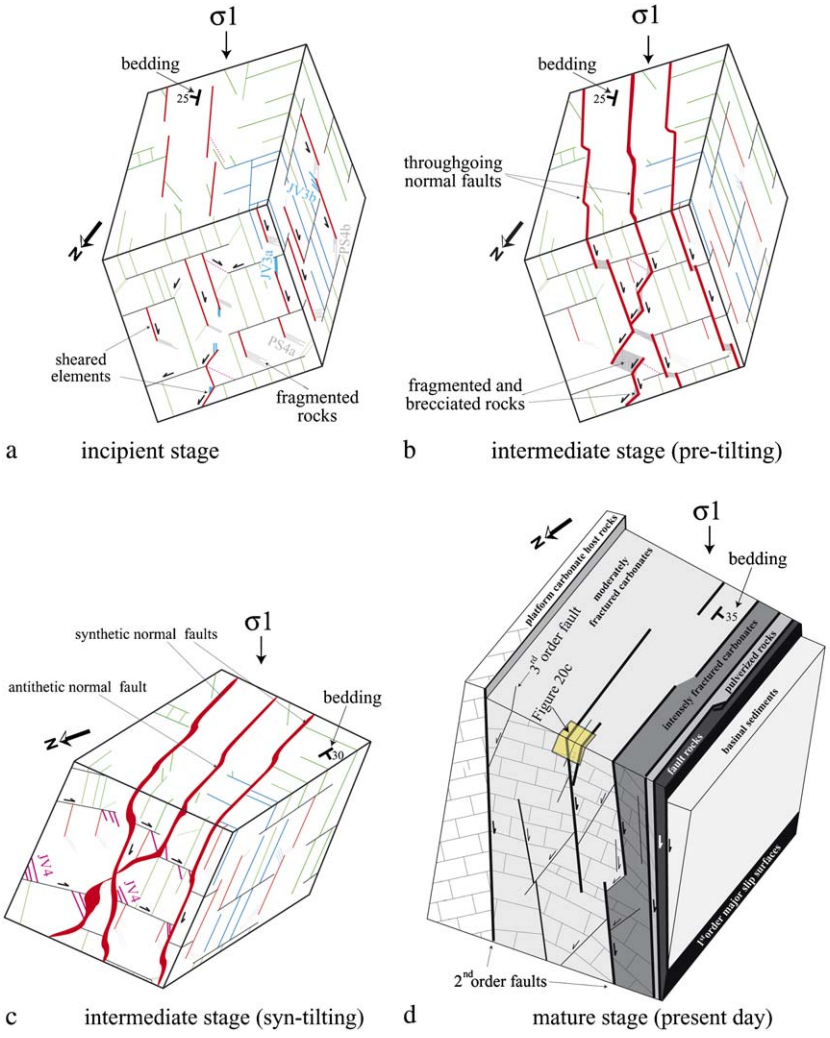

Fig. 20. Idealized block diagrams showing a model for normal fault development in platform carbonates. (a) Meter-long portion of the block diagram shown in Fig. 19c. Shearing of the pre-existing structured and formation of tail pressure solution seams, PS4a and PS4b, and tail joints and veins, JV3a and JV3b. The coalescence of these tail fractures with the pre-existing elements formed fragmented zones within the PS1-bounded mechanical layers. (b) Linkage of the fragmented zones across adjacent mechanical layers and development of two sets of NW striking normal faults dipping SW and NE, respectively. (c) During ongoing slip, exhumation, and basinward tilting of the fault zone, normal shearing of the pressure solution seams, PS1, and development of tail joints/veins, JV4. The synthetic faults are hundreds of meters-long features with several centimeters thick cemented and uncemented fault rocks, slip surfaces coated with calcite, and a few meters thick damage zone. (d) Block diagram showing the current architecture of the Venere fault zone; the length is not in scale. The last stage of faulting is characterized by the juxtaposition of the basinal sediments of the hanging wall against the deformed carbonates of the footwall. The fault zone includes a fault core, with fault rocks and first-order slip surfaces, and a damage zone comprised of three domains with different deformation intensity (cf. Fig. 3a) and various dip domains (cf. Fig. 3b). The earlier structures are preserved in the relative less-deformed parts of the damage zone (cf. c).

Acknowledgements

Thanks to Dave Pollard, David Peacock, and Fabrizio Storti for comments and suggestions that helped us to improve the quality of this paper. We are in debt with Andrea Billi for the grain size distribution analysis of the rock samples. Thanks to Marco Antonellini, Mario Agosta, and Francesco Longo for their help during the different stages of fieldwork, and to Emanuele Tondi and Ghislain de Joussineau for the discussions on the processes of fault growth. Thanks to Mr. Santilli for providing us access to the quarry, and to the people of the cartographic office of the Abruzzo Region in L'Aquila for the kind help. This research was supported by the Rock Fracture Project at Stanford. Part of F.A.'s fieldwork was supported by a Stanford McGee grant.

References

Agosta, F., Kirschner, D.L., 2003. Fluid conduits in carbonate-hosted seismogenic normal faults of Central Italy. Journal of Geophysical Research 108 (B4), 2221, doi:10.1029/2002JB002013.

Agosta, F., Prasad, M., Aydin, A., in press. Physical properties of carbonate fault rocks, Fucino basin, central Italy: implications for fault seal in platform carbonates. Geofluids.

Alvarez, W., Engelder, T., Geiser, P.A., 1978. Classification of solution cleavage in pelagic platform carbonates. Geology 6, 263–266.

Antonellini, M., Aydin, A., 1994. Effect of faulting on fluid flow in porous sandstones: petrophysical properties. American Association of the Petroleum Geologists Bulletin 78, 355–377.

Antonellini, M., Aydin, A., Pollard, D., 1994. Microstructure of deformation bands in porous sandstones at Arches National Park, Utah. Journal of Structural Geology 16, 941–959.

Arthaud, F., Mattauer, M., 1970. Exemples de stylolites d'origine tectonique dans le Languedoc, et leurs relations avec la tectonique cassante. Bulletin de la Societe Geologique de France 11, 738–744.

Aydin, A., 1978. Small faults formed as deformation bands in sandstone. Pure and Applied Geophysics 116, 913–930.

Aydin, A., 2000. Fractures, faults, and hydrocarbon entrapment, migration and flow. Marine and Petroleum Geology 17, 797–814.

Aydin, A., Borja, I.R., Eichhubl, P., 2006. Geological and mathematical framework for failure modes in granular rocks. Journal of Structural Geology 28, 83–98.

Bai, T., Maerten, L., Gross, M.R., Aydin, A., 2002. Orthogonal cross joints: do they imply a regional stress rotation? Journal of Structural Geology 24, 77–88.

Basili, A., Valensise, G., 1991. Contributo alla caratterizzazione della sismicita' dell'area marsicano-fucense. Aree Sismogenetiche e Rischio Sismico in Italia, ING-SGA (Ed.), 197–214.

Berg, S.S., Skar, T., 2005. Controls on damage zone asymmetry of a normal fault zone: outcrop analysis of a segment of the Moab fault, SE Utah. Journal of Structural Geology 27, 1803–1822.

Billi, A., 2005. Grain size distribution and thickness of breccia and gouge zones from thin (<1m) strike-slip fault cores in limestones. Journal of Structural Geology 27, 1823–1827.

Bigi, G., Cosentino, D., Parotto, M., Sartori, R., Scandone, P., 1992. Structural Model of Italy, scale 1:500, 000, 6 sheets. CNR, Quaderni di Ricerca Scientifica 114.

Blenkinsop, T.G., 1991. Cataclasis and processes of particle size reduction. Pure and Applied Geophysics 136, 59–86.

Boschi, E., Guidoboni, E., Ferrari, G., Valensise, G., 1997. Catalogo dei forti terremoti in Italia dal 461 A.C. al 1990. ING-SGA (Ed.), pp. 644.

Bosi, C., 1975. Osservazioni preliminari su faglie probabilmente attive nell'Appennino centrale. Bollettino della Societa Geologica Italiana 94, 827–859.

Bosi, C., Messina, P., 1991. Ipotesi di correlazione fra successioni morfo-litostratigrafiche Plio-Pleistoceniche nell'Appennino laziale-abruzzese. Studi Geologici Camerti Special Volume 1991/2, 257–263.

Bosi, C., Galadini, F., Messina, P., 1995. Stratigrafia Plio-Pleistocenica della conca del Fucino. Il Quaternario 8, 89–93.

Caine, J.S., Evans, J.P., Forster, C.B., 1996. Fault zone architecture and permeability structure. Geology 24, 1025–1028.

Cartwright, J.A., Trudgill, B., Mansfield, C.S., 1995. Fault growth by segment linkage: an explanation for scatter in maximum displacement and trace length data from Canyonlands Grabens of SE Utah. Journal of Structural Geology 17, 1319–1326.

Cavinato, G.P., Carusi, C., Dall'Asta, M., Miccadei, E., Piacentini, T., 2002. Sedimentary and tectonic evolution of Plio-Pleistocene alluvial and lacustrine deposits of Fucino Basin (central Italy). Sedimentary Geology 148, 29–59.

Chester, F.M., Logan, J.M., 1986. Composite planar fabric of gouge from the Punchbowl fault, California. Journal of Structural Geology 9, 621–634.

Chester, F.M., Evans, J.P., Biegel, R.L., 1993. Internal structure and weakening mechanisms of the San Andreas faults. Journal of Geophysical Research 98, 771–786.

Cowie, P.A., Scholz, C.H., 1992. Growth of faults by accumulation of seismic slip. Journal of Geophysical Research 97, 11085–11095.

Davatzes, N.C., Aydin, A., 2003. The formation of conjugate normal fault systems in folded sandstone by sequential jointing and shearing, Waterpocket Monocline, Utah. Journal of Geophysical Research 108 (B10), 2478,, doi:10.1029/2002JB002289.

Fletcher, R., Pollard, D., 1981. Anticrack model for pressure solution seams. Geology 9, 419–424.

Galadini, F., Galli, P., 1999. The Holocene paleo-earthquakes on the 1915 Avezzano earthquake faults (central Italy): implications for active tectonics in the central Apennines. Tectonophysics 308, 143–170.

Gasparini, C., Iannacone, G., Scarpa, R., 1985. Fault-plane solutions and seismicity of the Italian peninsula. Tectonophysics 117, 59–78.

Gawthorpe, R.L., Jackson, C., Young, I.M.J., Sharp, R., Moustafa, A.R., Leppard, C.W., 2003. Normal fault growth, displacement localization and the evolution of normal fault population: the Hammam Faraun fault block Suez rift, Egypt. Journal of Structural Geology 25, 88–895.

Ghisetti, F., Vezzani, L., 1999. Depth and modes of Pliocene-Pleistocene crustal extension of the Apennines (Italy). Terra Nova 11, 67–72.

Ghisetti, F., Kirschner, D.L., Vezzani, L., Agosta, F., 2001. Stable isotope evidence for contrasting paleofluid circulation in thrust and seismogenic normal faults of central Apennines, Italy. Journal of Geophysical Research 106, 8811–8825.

Giraudi, C., 1989. Lake levels and climate for the last 30,000 years in the Fucino area (Abruzzo, central Italy)- a review. Palaeogeography, Palaeoclimatology, Palaeoecology 70, 249–260.

Graham, B., Antonellini, M., Aydin, A., 2003. Formation and growth of normal faults in carbonates within a compressive environment. Geology 31, 11–14.

Graham, B., Girbecca, R., Mesonjesi, A., Aydin, A., in press. Evolution of fluid pathways through fracture controlled faults in carbonates of the Albenides fold-and-thrust belt. American Association of Petroleum Geologists Bulletin.

Groshong, R.H., 1988. Low-temperature deformation mechanisms and their interpretation. Geology Society of America Bulletin 100, 1329–1360.

Hubbert, M.K., Rubey, W.W., 1959. Role of fluid pressure in the mechanics of overthrusting faulting. Geological Society of America Bulletin 70, 115–166.

Kelly, P.G., Peacock, D.C.P., Sanderson, D.J., 1998. Linkage and evolution of conjugate strike-slip fault zones in platform carbonates of Somerset and Northumbria. Journal of Structural Geology 20, 1477–1493.

Kim, Y.S., Peacock, D.C.P., Sanderson, D.J., 2004. Fault damage zones. Journal of Structural Geology 26, 503–517.

Krumbein, W.C., Pettijohn, F.C., 1938. Manual of Sedimentary Petrography. Appleton-Century-Crofts Inc, New York.

Marshak, S., Geiser, P.A., Alvarez, W., Engelder, T., 1982. Mesocopic fault array of the northern Umbrian Apennine fold belt: geometry of conjugate shear by pressure-solution slip. Geological Society of America Bulletin 93, 1013–1022.

Martel, S.J., Pollard, D., Seagall, P., 1988. Development of simple strike-slip fault zones, Mount Abbot Quadrangle, Sierra Nevada, California. Geological Society of America Bulletin 100, 1451–1465.

Myers, R., Aydin, A., 2004. The evolution of faults formed by shearing across joint zones in sandstones. Journal of Structural Geology 26, 947–966.

Micchetti, A., Brunamonte, F., Serva, L., Vittori, E., 1996. Trench investigations of the 1915 earthquake fault scarps (Abruzzo, central Italy): geological evidence of large, historical events. Journal of Geophysical Research 101, 5921–5936.

Mollema, P.N., Antonellini, M., 1999. Development of strike-slip faults in the dolomites of the Sella Group, northern Italy. Journal of Structural Geology 21, 273–292.

Nelson, R.A., 1981. Significance of fracture sets associated with stylolite zones. American Association of Petroleum Geologists Bulletin 65, 2417–2425.

Oddone, E., 1915. Gli elementi fisici del grande terremoto marsicano-fucense del 13 gennaio 1915. Bollettino della Societa' Geologica Italiana 19, 71–215.

Ohlmacher, G., Aydin, A., 1995. Progressive deformation and fracture patterns during foreland thrusting in the Southern Appalachians. American Journal of Science 295, 943–987.

Peacock, D.C.P., Sanderson, D.J., 1995. Pull-aparts, shear fractures and pressure solution. Tectonophysics 241, 1–13.

Petit, J.P., Mattauer, M., 1995. Paleostress superimposition deduced from mesoscale structures in limestone: the Matelles exposures. Languedoc, France. Journal of Structural Geology 17, 245–256.

Piccardi, L., Gaudemer, Y., Tapponnier, P., Boccaletti, M., 1999. Active oblique extension in the central Apennines (Italy); evidence from the Fucino region. Geophysical Journal International 2, 499–530.

Pollard, D., Aydin, A., 1988. Progress in understanding jointing over the past century. Geological Society of America Bulletin 100, 1181–1204.

Rispoli, R., 1981. Stress fields about strike-slip faults inferred from stylolites and tension gashes. Tectonophysics 75, 29–36.

Salvini, F., Billi, A., Wise, D.U., 1999. Strike-slip fault-propagation cleavage in carbonate rocks: the Mattinata fault zone, Southern Apennines, Italy. Journal of Structural Geology 21, 1731–1749.

Sibson, R.H., 1977. Fault rocks and fault mechanisms. Journal of the Geological Society of London 133, 191–213.

Srivastava, D.C., Engelder, T., 1990. Crack-propagation and pore-fluid conditions during fault-bend folding in the Appalachian Valley and Ridge, central Pennsylvania. Geological Society of America Bulletin 102, 116–128.

Storti, F., Billi, A., Salvini, F., 2003. Grain size distribution in natural carbonate fault rocks: insights for non-self-similar cataclasis. Earth and Planetary Science Letters 206, 173–186.

Twiss, R., Moores, E.M., 1992. Structural Geology. Freeman and Co, pp. 532.

Vezzani, L., Ghisetti, F., 1998. Carta geologica dell'Abruzzo. S.EL.CA, Firenze.

Willemse, E.J., Peacock, D.C.P., Aydin, A., 1997. Nucleation and growth of strike-slip faults in platform carbonates from Somerset, U.K. Journal of Structural Geology 19, 1461–1477.